Final Report
Thermal Radiation Characteristics and Thermophysical Properties of Lunar Materials

N74-75899

Unclas
54853

00/99

by
Richard Birkebak & Clifford Cremers
Department of Mechanical Engineering
University of Kentucky

Submitted by
University of Kentucky Research
Foundation
Lexington, Kentucky

July 1974

AUG 1974
RECEIVED
NASA STI FACILITY
INPUT BRANCH

(NASA-CR-139950) THERMAL RADIATION CHARACTERISTICS AND THERMOPHYSICAL PROPERTIES OF LUNAR MATERIALS Final Report (Kentucky Research Foundation) 85 p

Final Report

THERMAL RADIATION CHARACTERISTICS AND THERMOPHYSICAL PROPERTIES OF LUNAR MATERIALS

This is the final report of work performed on NASA Contract NAS9-8098 and grants NGR18-001-060 and 18-001-026.

The report consists of a two-part review which summarize our measurements and those of others on lunar thermophysical properties and heat transfer within the lunar surface.

The resulting work has resulted in 30 publications in the open literature. Most of these are referenced in the literature surveys of Parts I and II. In addition to the reported measurements, Apollo 17 results are being published elsewhere.

Richard Birkebak
Clifford Cremers

Reprinted from:
ADVANCES IN HEAT TRANSFER, VOL. 10
© 1974
ACADEMIC PRESS, INC.

Thermophysical Properties of Lunar Materials: Part I

THERMAL RADIATION PROPERTIES OF LUNAR MATERIALS FROM THE APOLLO MISSIONS

RICHARD C. BIRKEBAK

Department of Mechanical Engineering, University of Kentucky, Lexington, Kentucky

I. Introduction 1
II. Apollo Samples: Location and Description 4
III. Remote Sensing Results 7
IV. Thermal Radiation Measurements 12
A. Definitions 13
B. Measurement Techniques 16
C. Experimental Results 19
V. Summary 34
Nomenclature 35
References 35

I. Introduction

For eons men have looked upon the moon, speculated about its nature, and wondered about its origin. Men have dreamed of visiting the lunar surface and have written books on their speculations. The Apollo program has culminated these aspirations and made them a reality. The landing of men on the lunar surface and subsequent return of lunar samples has led and is leading to a better understanding of the origin of the solar system and moon–earth system.

There have been a number of soft landings on the moon in the past several years including five unmanned Surveyor flights and five manned Apollo flights by the United States, and several unmanned Luna flights by

the Soviet Union.[1] Several of these missions included provision for measurement of lunar surface temperatures and heat fluxes. Ironically, the first flight which included such experiments was the Apollo 13 flight which was aborted before a landing could take place. A successful heat flow experiment was installed by the Apollo 15 crew at Hadley Rille and it returned the first direct measurements of heat flux and temperature from the moon. An unfortunate accident by one of the Apollo 16 astronauts terminated the Apollo 16 heat flow experiment. The other actual measurements of lunar temperatures have been remote measurements from earth in which infrared or microwave radiation emitted by the dark moon, either at lunar nighttime or during an eclipse, was analyzed to yield an apparent radiation temperature.

The successful landings on the moon of the Apollo flights and the return of samples of lunar surface material has permitted the measurement of the thermophysical properties necessary for heat transfer calculations. These explorations have also proven what was previously hypothesized from remote thermal radiation measurements and laboratory studies [1], that the lunar surface is covered to a depth of several meters or more, at least in the mare regions, with a layer of fine particulate soil. There is a hard substratum below these "fines" and there are many rocks and sometimes boulders scattered about as well. However, these occur randomly and may be considered perturbations in the porous, powdery surface layer [2, 3].

Man has learned much about the moon's optical properties, temperature, surface features, and thermophysical properties by using remote sensing techniques from astronomical, infrared, microwave, and radar measurements. The returned lunar samples are allowing scientists to compare physical properties obtained directly from these samples with those inferred from remote sensing results.

The thermal radiation properties described herein have and are being used in heat transfer calculations [4–7] for the prediction of lunar surface temperatures, spacecraft temperatures, and temperature variation of scientific equipment placed on the lunar surface. The proper design and operation of such systems or structures which may be constructed for the lunar surface depend to a large degree on a complete knowledge of the thermal transport properties of the material in the lunar surface layer. Accurate data on the local thermal environment are also needed, particularly on the moon where there are wide extremes of temperature. However, up to the Apollo 15 mission there has not been any direct measurements of

[1] Subsequent to the writing of this paper the Apollo 17 mission was successfully completed. The returned lunar material is now being studied.

the temperature field in the surface layer, nor had there been any reports until recently of the actual properties of the lunar material.

We became involved in the Lunar Sample Analysis Program of the National Aeronautics and Space Administration in October 1966 when our group was selected as one of the initial 110 groups to study lunar material. Our group was selected to measure the thermophysical properties of lunar materials. This article reviews our results and those of other investigators on the thermal radiation properties of lunar material returned by the Apollo 11, 12, 14, and 15 missions and also, where possible, compares these results with remote sensing data.

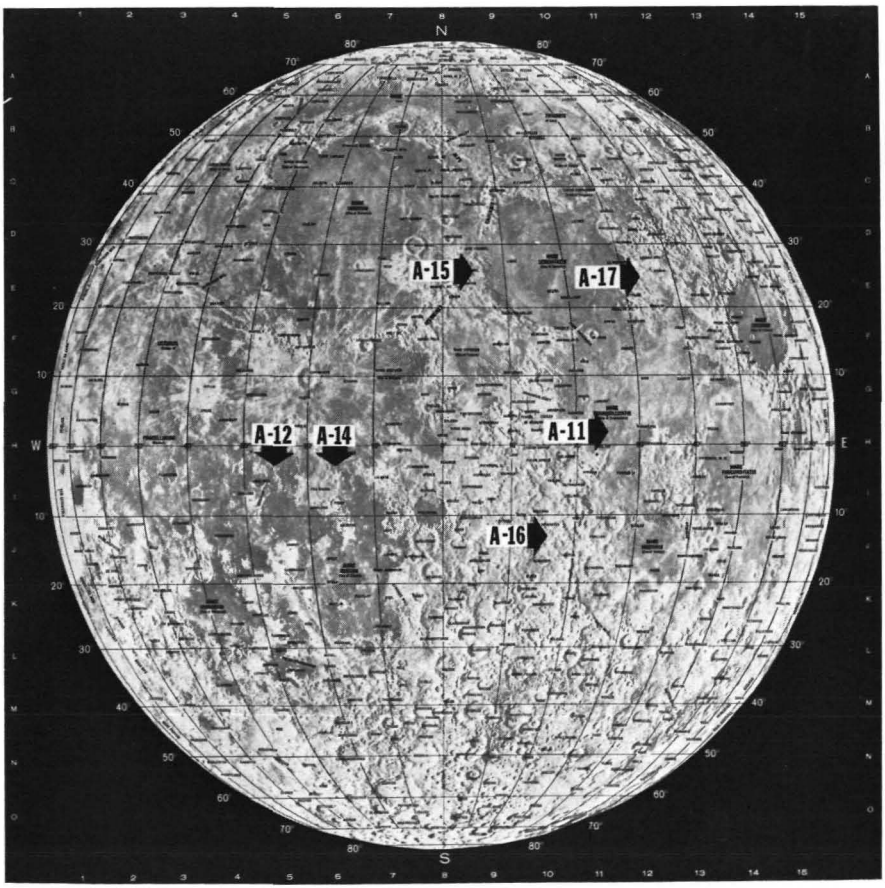

FIG. 1. Apollo mission landing sites (NASA).

II. Apollo Samples: Location and Description

On July 20, 1969, astronaut Armstrong stepped onto the lunar surface in the Sea of Tranquility at the location 0.67°N and 23.49°E. This site is shown on the photograph of the lunar surface, Fig. 1. During the extravehicular activity (EVA) phase the astronauts collected about 21.5 kg of lunar material. About one-half of the returned lunar material was fine-grained soil (called fines) and half was selected rock fragments. All of the samples were collected near the lunar module in an area approximately 7 × 22 meters. A complete description of the Apollo 11 samples is found in the *Proceedings of the Apollo 11 Lunar Science Conference* [2].

Each lunar specimen as cataloged by NASA's Lunar Receiving Laboratory is specified by a number which identifies the Apollo mission and sample. A five-digit number is used, succeeded by two or three more digits; this refers to a particular split of the main sample. Documented sample histories include in many cases the sample location and orientation on the surface of the moon. The sample series begin with 10000, 12000, and 14000 referring to samples from the Apollo 11, 12, and 14 missions, respectively.

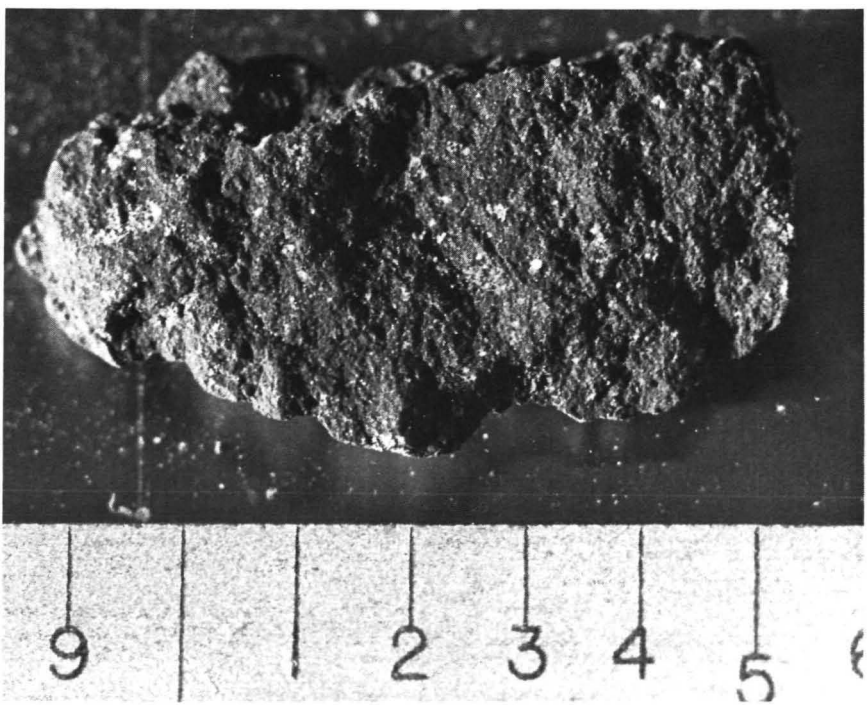

FIG. 2. Apollo 11 rock chip 10047.

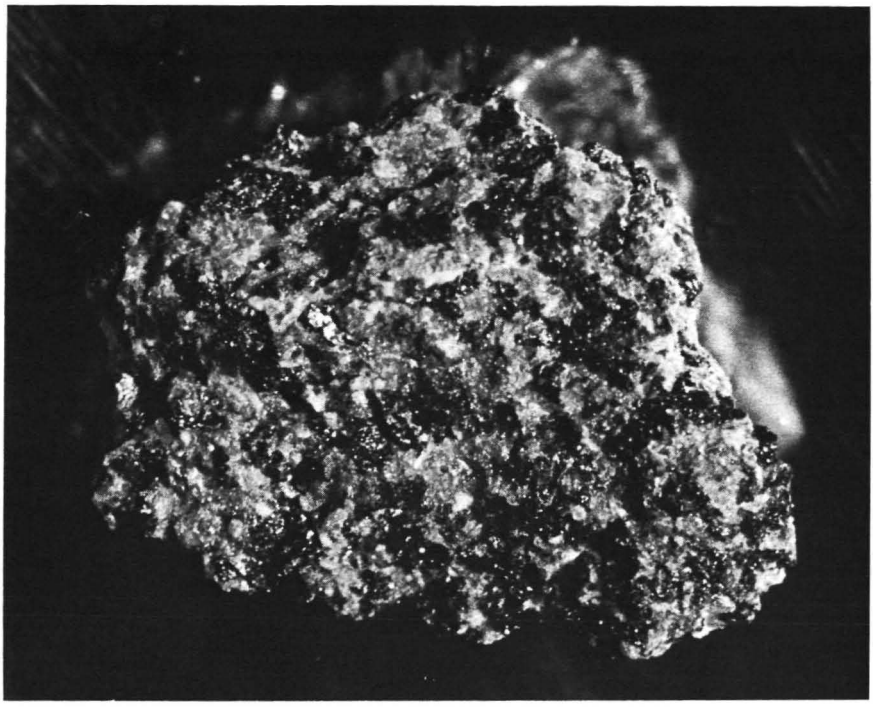

FIG. 3. Apollo 11 rock chip 10048.

Photographs of three rock chips from the Apollo 11 mission are shown in Figs. 2–4, and illustrate the variation in textural nature of the rocks. These chips are from larger parent rocks. Rock number 10047 is a coarse-grained, vuggy, ophitic cristobalite basalt [2], 10048 a breccia [2], and 10057 a fine-grained, vesicular to vuggy, granular basalt [2].

The Apollo 11 lunar fines consisted of a distribution of small crystalline fragments and glassy fragments with a variety of shapes. Particle sizing of the fines [8] showed a range from 200 μm down to less than 1 μm, with most of the particles being at the small diameter end of the range. Much larger rock fragments were in the initial soil sample but were removed prior to this study [8]. The other Apollo fines have similar distributions when compared to that of Apollo 11 fines.

The second manned lunar landing mission, Apollo 12, landed on the Ocean of Storms with coordinates 3.0°S latitude and 23.4°W longitude on November 19, 1969 [3]. During this mission two EVA's were carried out which explored the lunar surface. Approximately 34 kg of material was collected with 82% being rock samples and the remainder of fines.

The third lunar landing was made at Fra Mauro at latitude 3.66°S,

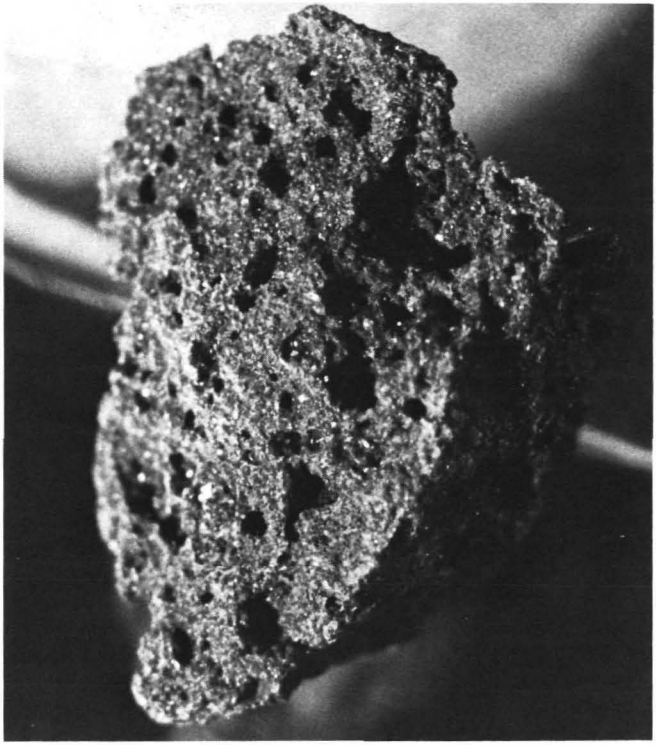

FIG. 4. Apollo 11 rock chip 10057.

longitude 17.48°W by the Apollo 14 lunar module on February 4, 1971. This mission provided an exceptionally rich harvest for lunar science. The Apollo 14 crew returned 43 kg of lunar material. The Apollo 14 samples may be contrasted with the samples returned from the Mare Tranquillitatis and the Oceanus Procellarum in that their chemical composition is quite different, and the Apollo 14 rocks exhibit characteristics that suggest they are ejects from the Imbrium Basin [9].

On July 30, 1971 the Apollo 15 mission, the fourth in the series, landed in the Hadley-Apennine region of the moon at a latitude of 26.1°N and longitude of 3.65°E [10].

Four EVA's were performed on the lunar surface and for the first time a lunar Rover was used to transport the astronauts. Astronauts Scott and Irwin brought back 77 kg of samples from the Hadley region [10].

To date, the oldest lunar material returned were the soils and breccias from Apollo 11 with ages of approximately 4.6 billion years [2]. The rocks

from Apollo 11 were younger by one billion years. In the oldest Apollo 12 material, the soils are one billion years younger than the Apollo 11 samples.

III. Remote Sensing Results

Prior to the Apollo, Surveyor, and Luna missions the only way that the surface of the moon was studied was by remote means, i.e., by optical and radar astronomical measurements. From those remote sensing results it has been possible to deduce many of the thermophysical properties of the lunar surface [1].

Hapke [1] reviews the optical remote sensing results prior to 1970 that appear in the literature. The general conclusions that he makes, and that are well known to people working in this area, are the five following characteristics.

(1) The moon has a low albedo with an average value of near 7%.

(2) The spectral albedo increases monotonically from 0.3 to 2.5 μm but has small and sometimes distinct variations in the spectrum.

(3) The lunar surface backscatters strongly, i.e., the moon's brightness peaks strongly at full moon when the sun is almost directly behind the observer.

(4) The degree of polarization of the lunar surface changes with phase angle (the angle between the observer and moon and sun) in a distinct manner.

(5) The previous four statements hold for every type of surface feature on the moon.

The most significant remote sensing results that have been reported to date are by McCord and Johnson [11, 12], McCord *et al.* [13], and Adams and McCord [14]. These data are the results of very careful experimental work. The ubiquity of the results over the lunar surface as stated in conclusion (5) is probably due to the fact that almost the entire lunar surface is covered with fines, but this does not mean that signification differences do not occur. The remote sensing data for normalized spectral reflectance is shown in Fig. 5. The results were measured for regions on the moon of approximately 18 km in diameter. Starting from the top curve and proceeding downward the results are for (a) the upland or highlands region, (b)–(d) the mare regions, (e) the upland bright craters, and (f) and (g) bright mare craters on the lunar surface. The curves have the form or trend as described in conclusion (1), however, there are significant differences. All curves indicate an absorption band near or at 0.95 μm. This band is due to clinopyroxene in the lunar fines and exposed rocks, and the depth of

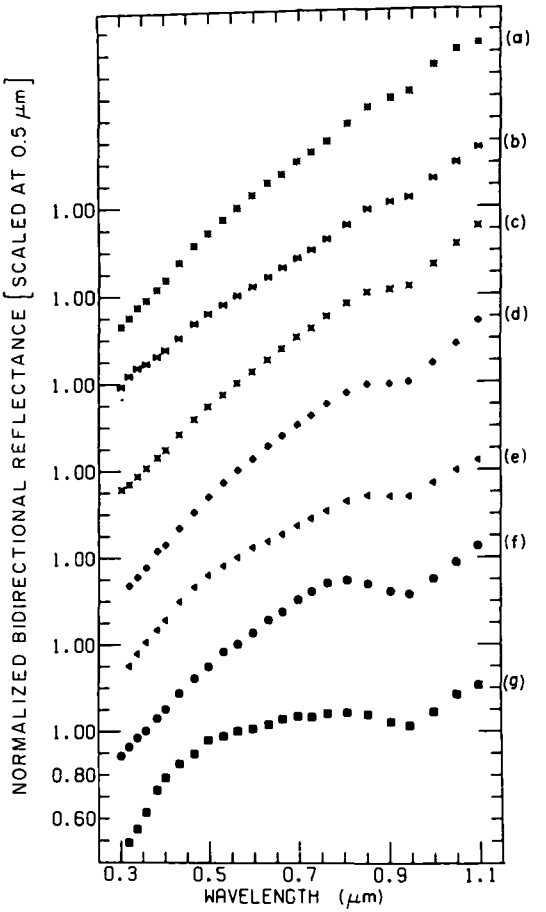

FIG. 5. Normalized bidirectional spectral reflectance (taken from McCord *et al.* [13]): (a) Sea of Moisture; (b) Sea of Tranquility; (c) Sea of Serenity; (d) Sea of Cold; (e) Tycho; (f) Sea of Moisture; (g) Aristarchus.

these bands is an indication of the amount of this mineral [14]. The slope of the curves is a function of the chemical composition of the lunar material and the amount of breccia and glass fragments in the fines [14]. McCord *et al.* [13] have normalized these results to a selected area in the Sea of Serenity. By doing this they have been able to emphasize spectral differences. The data in Fig. 5 have been normalized in this matter and the results are shown in Fig. 6. Clearly evident are different spectral types. From this type of procedure the composition and age of a given area on the moon can be inferred.

Adams and McCord [14] have shown that the spectral reflectance for the Sea of Tranquility obtained by remote sensing agrees well with that obtained in the laboratory. The laboratory data also enabled McCord *et al.* [13] to correct their remote sensing results for atmospheric absorption, etc. The comparison of these results is shown in Fig. 7.

According to Hapke [1] the most accurate presently available integral phase function distribution of reflected light from the moon was measured by Rougier [15]. A plot of his results is shown in Fig. 8. The normalized photometric distribution is presented as a function of phase angle. (In

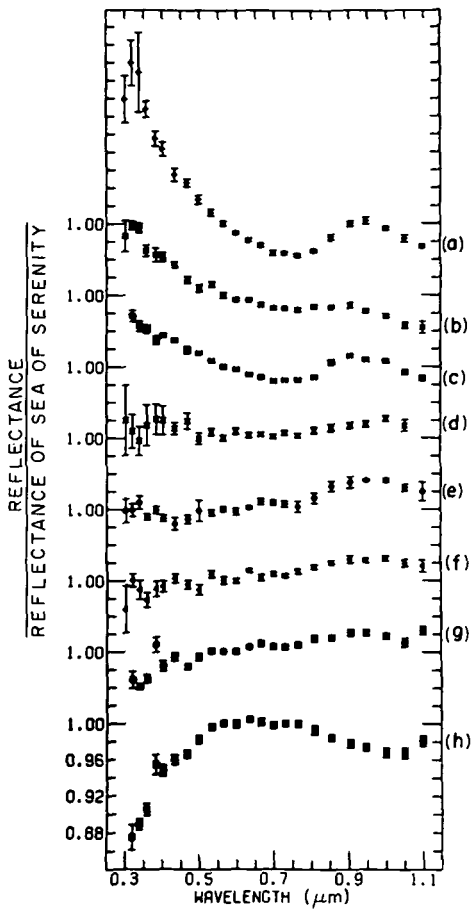

FIG. 6. Ratio of the reflectance of a lunar area to the Sea of Serenity (taken from McCord *et al.* [13]): (a) Sea of Tranquility, (b) Sea of Moisture, (c) Luna 16 landing site, (d) Fra Mauro, (e) Le Monnier, (f) Sea of Moisture, (g) Plato, (h) Sea of Cold.

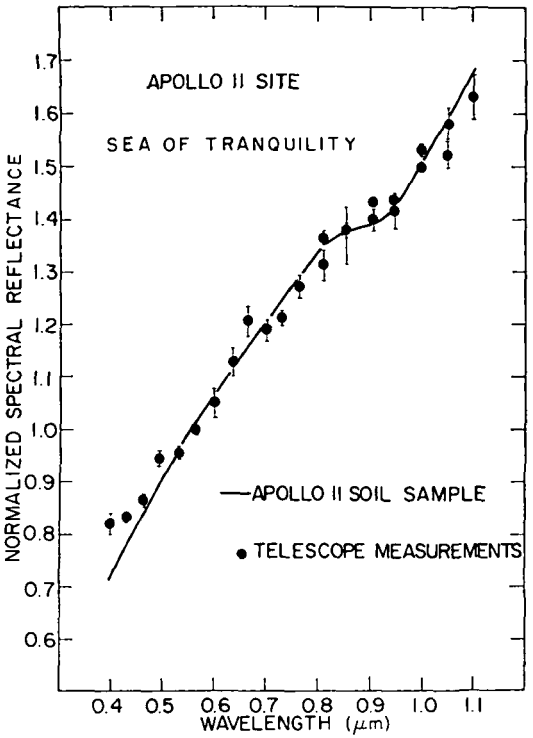

FIG. 7. Comparison of telescopic and laboratory-obtained reflectances for the Sea of Tranquility.

engineering practice we would refer to these as normalized bidirectional reflectances.) The lunar surface strongly backscatters the incident beam of sunlight. Hapke [16] formulated a theory that predicted this effect. Later improvements were made by Morozhenko and Yanovitskii [17]. In arriving at his theory, Hapke assumed that the lunar material had a "fairy-castle structure"; i.e., the grains of the soil stuck together in such a manner that the overall structure was very porous so that light could penetrate from any direction. From remote sensing results and laboratory studies on simulated lunar material, Hapke as well as others came to the conclusion that the surface of the moon was covered mainly with very small particles. This was eventually borne out by the analyses of the returned lunar samples and photographs returned of the lunar surface from the Apollo, Surveyor, and Luna missions.

As difficult as it is in the visible portion of the spectrum to obtain reliable remote sensing data, the problem in the infrared is even more so. The total

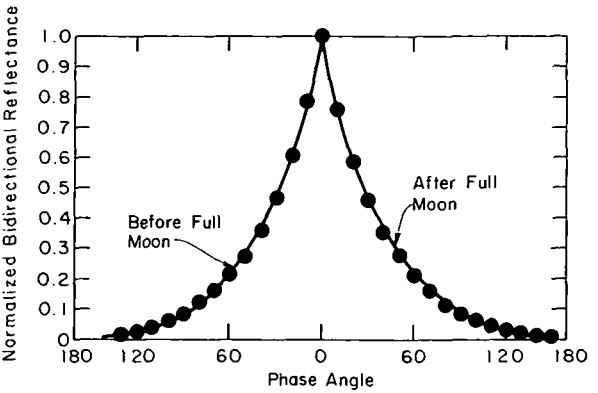

FIG. 8. Normalized bidirectional reflectance function.

emittance of the lunar surface has been usually assumed to be unity, a blackbody. However, the remote sensing results of Murcray [18] and Murcray *et al.* [19] made from a mountain top and from balloons gave data that showed that the moon was not a blackbody. A result of theirs is shown in Fig. 9 for a spectral range from 7.0 to 13.5 μm. These results will be discussed later. If it were possible to obtain reliable emittance data, especially where the maximum value occurs [20], then one could determine something about the mineralogy of the lunar surface. The maximum emittance location has been shown by Salisbury *et al.* [20] and Conel [21] to depend on the chemical composition of the substances that make up a powered material.

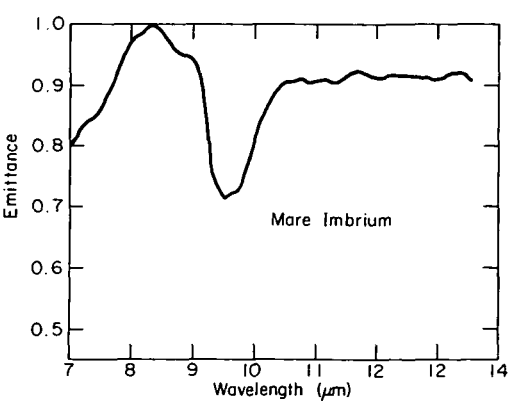

FIG. 9. Remotely obtained spectral emittance of Mare Imbrium.

IV. Thermal Radiation Measurements

During the lunar day the dominating or controlling parameters that affect the temperature of the lunar surface or objects on the surface are the thermal radiation characteristics of the lunar material. These characteristics include the bidirectional and directional reflectance and emittance of the lunar surface. It has been shown in Cremers *et al.* [6] that the directional solar albedo has the greatest effect on lunar surface temperature than any other single thermophysical property. This variable reflectance effect is clearly shown in Fig. 10 where the temperatures differ substantially just after sunrise and before sunset. Table I compares the constant and variable property results for specific lunation times. The maximum differences occurs for a lunation fraction of 0.24 and 0.76 where the variable property calculated temperatures are 43.7°K and 64.1°K lower, respectively.

In addition to the necessity of knowing the thermal radiation characteristics for heat balance calculations, they also are useful in remote sensing work as shown in the previous section. The spectral signature of a substance can be used to identify, in part, its mineral constituents; that is, the location of absorption bands in reflectance curves can usually be associated with a given mineral. And the determination of the spectral

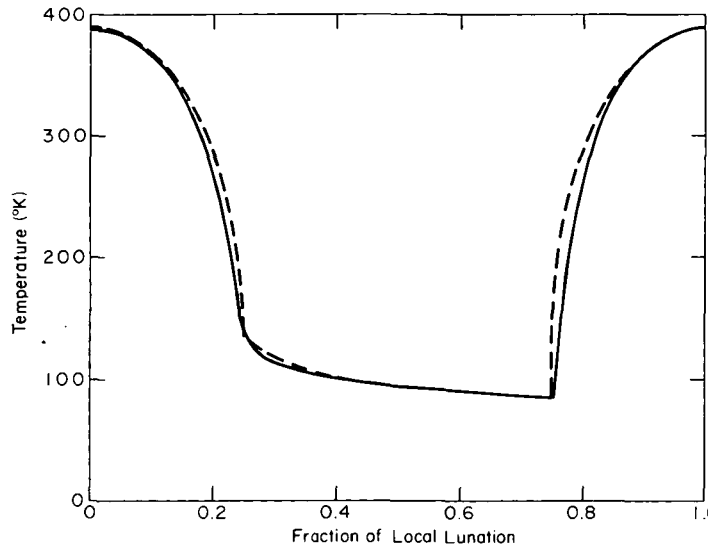

FIG. 10. Lunar surface temperature variation. —— Variable $\rho(\theta)$, $\epsilon(T)$, - - - constant ρ and ϵ.

reflectance gives us both thermal data as well as some spectral signature data as to the mineralogy of the material.

A. DEFINITIONS

In the literature on the photometry measurements on the moon one finds at least four different kinds of reflectances (albedos) used. Because the moon is a spherical body, it is natural that there arise albedos that take this into account. These definitions are presented here for the convenience of the reader.

1. *Bond Albedo*

The ratio of the amount of light reflected by a spherical body in all directions to that incident on the body is defined as the *Bond albedo, B.*

2. *Geometric Albedo*

As is often the case in photometry, albedo is defined in terms of a Lambertian surface. The *geometric albedo p* is the ratio of the brightness [radiance] of a body at zero phase angle to the brightness (radiance) of a Lambertian disk of the same angular diameter as the body and perpendicular to the sun's rays. The phase angle V, is the included angle between the source, sample, and observer.

These two albedos are related to each other by the following equations:

$$B = q \cdot p \tag{1}$$

where

$$q = 2 \int_0^{\pi} \Phi(V) \sin V \, dV \tag{2}$$

TABLE I

COMPARISON OF TEMPERATURE FOR CASE OF VARIABLE SURFACE PROPERTIES WITH THAT OF CONSTANT SURFACE PROPERTIES[a]

Fraction of lunation, τ	Temp. (°K) variable $\rho(\tau)$, $\epsilon(T)$	Constant[b] ρ, ϵ
0 (Noon)	389.3	389.4
0.24	161.2	204.9
0.25 (Sunset)	134.4	147.5
0.50 (Midnight)	94.7	96.8
0.75 (Sunrise)	86.1	87.8
0.76	125.4	189.5

[a] Cremers *et al.* [6]. [b] Cremers *et al.* [5].

and the quantity $\Phi(V)$ is called the integral phase function. It describes the manner in which the light from the lunar surface is distributed. The function $\Phi(V)$ is taken to be 1 at $V = 0$.

3. *Normal Albedo* (A)

If the curvature effects are eliminated, that is, if we consider a flat surface, the analogy to the geometric albedo is the *normal albedo* (A). It is the brightness of an area at an arbitrary angle of illumination, to the brightness of a Lambertian disk under the same solid angle but at zero angle of illumination. This albedo is the most frequent one reported because of the following reason. The photometric distribution function of the lunar surface behaves in such a manner that the normal albedo is independent of the direction of illumination and viewing.

The fourth albedo found in the literature is the analogy to the spherical Bond albedo, it is the hemispherical albedo. This albedo is the same as the directional reflectance described next.

4. *Directional Reflectance*

The *directional reflectance* is used mainly in the calculation of the heat balance and temperatures of the lunar surface. It is defined in the following manner:

Let the incident radiation be contained in a solid angle $\Delta\Omega_i$ oriented at a specific angle Ψ relative to the surface normal (Fig. 11a), and let reflected radiation be collected over the entire hemispherical space above the surface. We then define the directional hemispherical reflectance as

$$\rho(\Psi) = de_{r,h}/de_i(\Psi) \tag{3}$$

where $de_{r,h}$ is the reflected radiant energy that is collected over the entire hemispherical space and de_i is the radiant energy contained in the incident beam. In general, the magnitude of $de_{r,h}$ will depend upon the angle of illumination Ψ of the incoming beam.

The directional reflectance can also be understood to mean the following. Let the surface under study be illuminated hemispherically with diffuse radiation $e_{i,h}$ while the reflected radiance $i_r(\theta)$ is collected in a small solid angle $\Delta\Omega_r$ (Fig. 11b). The hemispherical directional reflectance is defined as

$$\rho(\theta) = i_r(\theta)/(e_{i,h}/\pi) \tag{4}$$

With the use of reciprocity, the reflectances in Eqs. (3) and (4) can be shown to be identical if the solid angles are the same, $\Delta\Omega_i = \Delta\Omega_r$.

$$\rho(\Psi) = \rho(\theta) \qquad \text{for} \quad \theta = \Psi \tag{5}$$

The measurement of $\rho(\theta)$ with the integrating sphere is called the reciprocal mode.

5. *Bidirectional Reflectance*

The angular distribution of reflected radiation from a surface can be described by the *bidirectional reflectance.* The bidirectional reflectance is defined as the ratio of the radiance of the reflected light in the direction of viewing θ to the incident energy per unit time and surface area contained within a solid angle $d\Omega_i$ in the direction Ψ,

$$\rho_b(\Psi, \theta) = \pi \, di_r(\Psi, \theta)/de_i(\Psi) \tag{6}$$

where di_r is the reflected radiance and $de_i(\Psi)$ is the incident flux of energy.

6. *Directional Emittance*

The directional spectral emittance of a sample is defined as the ratio of the radiance of radiation from the sample to radiance of radiation from a blackbody at the same temperature,

$$\epsilon(\theta, \lambda, T) = i_S(\theta, \lambda, T)/i_B(\lambda, T) \tag{7}$$

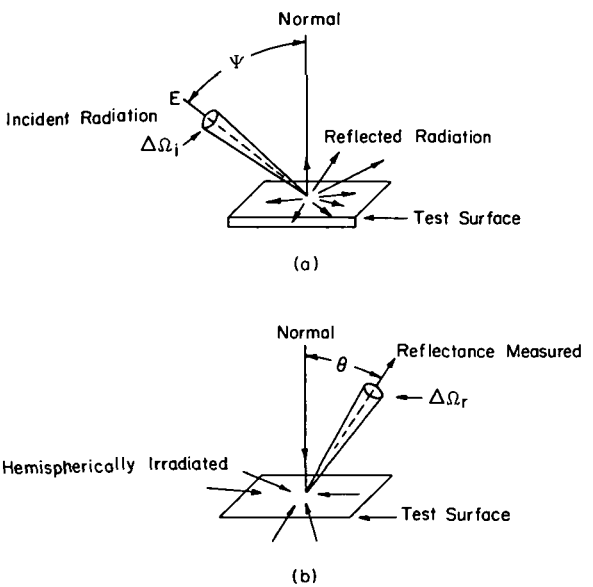

FIG. 11. Definition of coordinates: (a) directional hemispherical technique; (b) hemispherical directional technique.

where θ is the angle of viewing, T the temperature of the sample, and i_S and i_B are the radiance of the sample and blackbody, respectively.

These thermal radiation property definitions are used in the following sections to describe the radiation characteristics of the lunar material.

B. MEASUREMENT TECHNIQUES

In this section we will briefly describe the experimental techniques used by us to determine the thermal radiation characteristics of lunar material.

1. *Directional Reflectance Apparatus*

The directional reflectance was obtained with a sample, center mounted in an integrating sphere reflectometer. The sphere coating was magnesium oxide. The sphere system was constructed with the sample held in a horizontal position, a necessity for powders, while by rotation of the sphere and external optics, angles of illumination or viewing up to approximately 75° are obtained.

Since the theory of the integrating sphere is well known, it will be only briefly reviewed. Radiation directed on a test sample within the integrating sphere is reflected onto the sphere wall. If the wall is coated with a highly reflective and diffuse material, then any radiation hitting the wall is reflected diffusely throughout the sphere. The total radiation incident on a given area will be a summation of radiances from the multiple reflections. A detector mounted at the sphere wall measures radiance of the radiation striking a given area within the sphere.

Our integrating sphere was operated in the reciprocal mode, that is, the sample was illuminated by diffuse light from the sphere walls. The ratio of radiance when the center-mounted sample was viewed to the radiance when the wall was viewed is the directional reflectance $\rho(\theta)$ [Eq. (4)]. As represented in Eq. (5) this measurement is equivalent to illuminating the sample at an angle of incidence Ψ equal to the angle of viewing θ.

A sketch of the apparatus used in this research is shown in Fig. 12. The integrating sphere was constructed of stainless steel hemispheres, 0.20 m in diameter, flanged and joined by a copper gasket seal. The interior of the sphere was smoked with MgO until a uniform coating of 2 mm thickness was obtained. Ports were provided on the sphere for the test sample, detector optics, light source, and vacuum pump.

The actual sample transfer system [22] was constructed so that the sample could be located along the diametral plane of the sphere and always held in a horizontal position under vacuum condition. The sample size was 25 mm in diameter by 6.0 mm in depth.

The viewing optics were arranged so that the sample or sphere wall

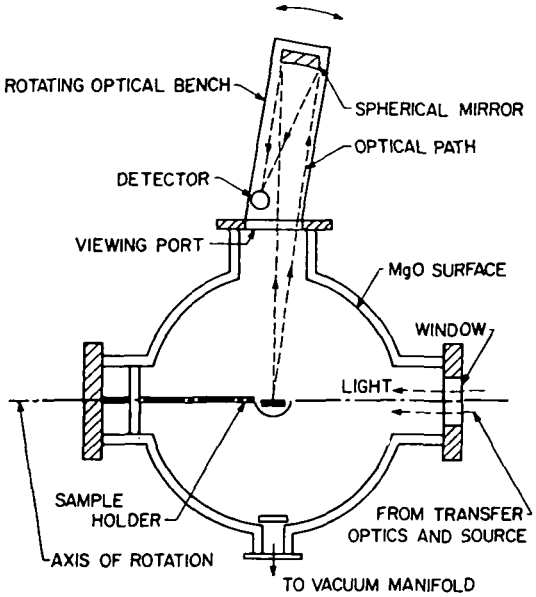

FIG. 12. Schematic of integrating sphere.

could be viewed by rotating the optical bench, Fig. 12. The spectral results were obtained with a Perkin–Elmer 112 U spectrometer having a tungsten–iodine source and a lead–sulfide detector. The total or white light measurements were made with a 1000-W tungsten–iodine lamp (DXW) with a reflector and with a Kipp–Zonen CA-1 thermopile. Details of the design and construction are presented in a technical report, Birkebak and Cremers [23]. The measurements were obtained automatically by joining the spectrometer and its associated electronics to a minicomputer.

2. *Bidirectional Reflectance Apparatus*

The bidirectional reflectance measurements were made with a goniometric system designed so that the samples could be viewed and illuminated while under vacuum conditions. A schematic of the apparatus is shown in Fig. 13. The energy from the sample is reflected from three diagonal mirrors before it emerges from the system. It is then focused onto the entrance slit of the spectrometer or onto a detector. For this system the surface could be illuminated at a fixed angle of illumination (Ψ) and the angle of viewing (θ) varied or, by reversing the optical path, the angle of illumination was varied and the angle of viewing was held fixed.

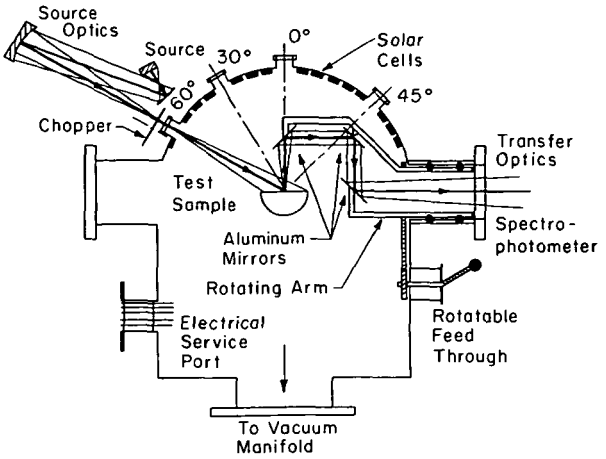

FIG. 13. Bidirectional reflectance system.

3. *Spectral Emittance Apparatus*

The nature of the sample dictated that we use a horizontal sample in the measurements. The sample was mounted in a sample heating cup and positioned in a known radiation environment as shown in Fig. 14. Besides the sample holder a heated reference blackbody was placed in the environment chamber. Transfer optics were used to view either the sample or blackbody and to direct the energy into a Perkin–Elmer 112 U spectrometer.

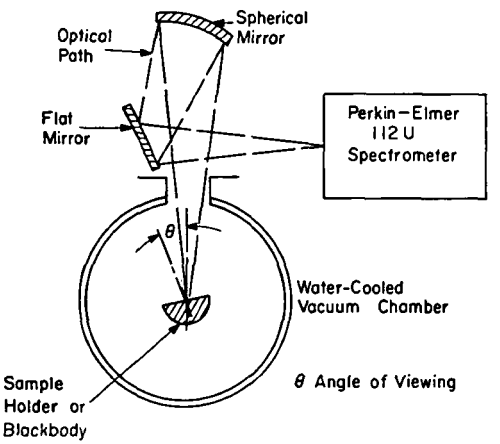

FIG. 14. Schematic of emittance system.

The spectrometer was interfaced with a Hewlett-Packard 2114B minicomputer. This system allowed us to automatically scan the wavelength range of interest and to perform the necessary operations required to obtain data. A complete discussion of the analysis of this technique is given elsewhere [24]. The working equation used by the system to obtain the spectral emittance is:

$$\epsilon(\theta, T) = \frac{\Delta(\mathrm{S}) - \Delta(\mathrm{R})}{\Delta(\mathrm{B}) - \Delta(\mathrm{R})} \frac{\exp[c_2/\lambda T_\mathrm{R}] - \exp[c_2/\lambda T_\mathrm{B}]}{\exp[c_2/\lambda T_\mathrm{R}] - \exp[c_2/\lambda T_\mathrm{S}]} \times \left\{\frac{\exp[c_2/\lambda T_\mathrm{S}] - 1}{\exp[c_2/\lambda T_\mathrm{B}] - 1}\right\} \tag{8}$$

where $\Delta(\mathrm{S})$, $\Delta(\mathrm{B})$, $\Delta(\mathrm{R})$ and T_S, T_B, T_R are the detector output and thermocouple readings for the sample, heated reference blackbody, and blackened surrounds, respectively.

C. Experimental Results

Before discussing the experimental results obtained on the returned lunar samples, the following facts should be kept in mind. A number of investigators have recognized that the density (packing, compactness) of the lunar fines will effect the measured properties [25–28]. However, only Birkebak *et al.* [26] actually specify the bulk densities used in their experiments. Hapke *et al.* [25] discuss the change in albedo with packing and describe various ways to change the material density but do not give any quantitative results for the density. From the description given in the various papers reviewed it appears that many of the investigators sifted or gently poured the lunar fines into their sample holders. We have carried out several experiments using these methods and find that the bulk density can range from approximately 900 to 1100 kg/m^3. However, these surfaces are very susceptible to vibrations and settle slowly.

1. *Bidirectional Reflectance Results*

As important as the knowledge of the bidirectional reflectance distribution is to the heat balance calculations on structures on the lunar surface, only a limited amount of data is available: In their original papers, Birkebak *et al.* [29a, b] and Gold *et al.* [8] and later, Gold *et al.* [27] and O'Leary and Briggs [30], present bidirectional reflectance results.

As discussed in Section III on remote sensing, the geophysicists presented their results for a fixed angle of observation and variable angle of illumination; whereas, in thermal property measurements we usually

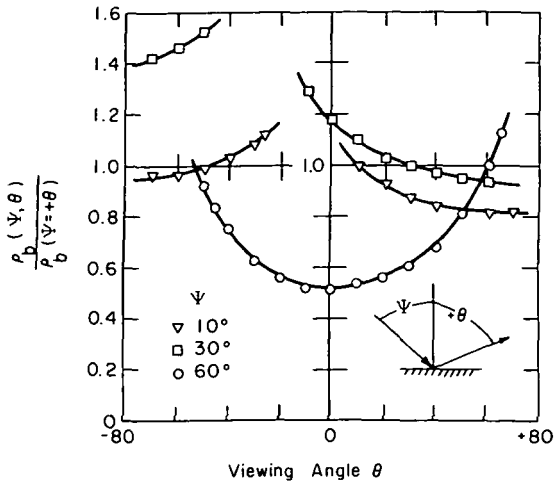

FIG. 15. Normalized bidirectional reflectance—Apollo 11 sample No. 10084.68.

present the bidirectional reflectances for a fixed angle of illumination and variable angle of viewing. Therefore, direct comparison is not possible of the two results obtained in the laboratory on lunar fines.

The results of Birkebak *et al.* [29a, b] are shown in Fig. 15. The sample was illumination with white light (1000-W tungsten–iodine lamp) at angles of 10°, 30°, and 60°. We have normalized the results with respect to the specular ray direction, $\Psi = +\theta$. A perfectly diffuse surface would give a horizontal line. It is quite apparent that the lunar material backscatters very strongly in the direction of illumination.

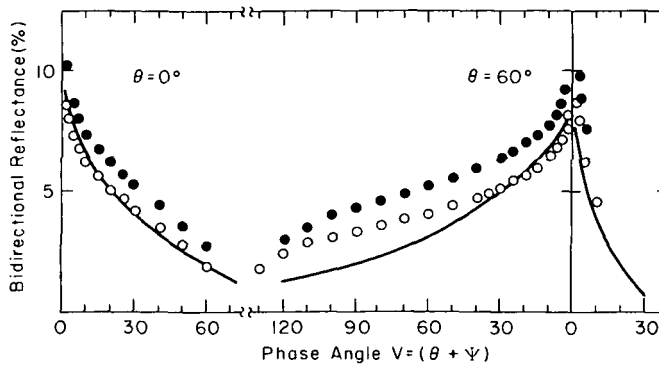

FIG. 16. Bidirectional reflectance as a function of phase angle V. Symbols: ●, Apollo 12 soil; ○, Apollo 11 soil; —, moon (normalized to Apollo 11); θ, angle of viewing; λ, 0.56 μm.

The backscatter peak could not be measured with our present equipment. However, the peak is estimated to have a value as high as 2–3. This explains why the moon appears so bright during opposition (zero phase angle). In the laboratory if one illuminates the lunar fines at an angle of 30° and then moves one's head over the hemispherical space above the surface, one can physically see this distribution of reflected light; a very interesting and rewarding experience. There is a slight wavelength effect that we have found and which has also been determined by O'Leary and Briggs [30]. As one approaches zero phase angle, and also for large phase angles, the color of the fines changes from a grayish-blue to a reddish hue.

The results of O'Leary and Briggs [30] and Gold *et al.* [27] are shown in Fig. 16. Their results of reflectance are plotted against phase angle. The solid curve is the moon remote sensing data [31] normalized with respect to the normal albedo of Apollo 11.

2. *Directional Reflectance Results*

We will first discuss directional reflectance made on lunar rock chips. Although these results are not useful in heat transfer calculations, they are useful in obtaining spectral signatures of the various minerals. Second, we will discuss the results obtained on the lunar fines, which, as we have stated previously, covers almost the entire moon to several meters or more in depth.

a. Lunar Rock Chips. The Apollo astronauts have brought back many rocks that weighed more than several kilograms. However, most investigators received only a small rock chip or thin section that weighed around 3.0 g. Because these chips were so small in size it was difficult to obtain representative reflectance results. Many of the returned rock had surfaces which could be identified from photographs as having been exposed to the lunar environment, and as a result one could sometimes readily see differences in surface properties. Adams and McCord [14], Birkebak *et al.* [29a, b], Adams and McCord [32], Conel and Nash [33], Gold *et al.* [8], Nash and Conel [34], and Perry *et al.* [35, 36] have all presented reflectance spectra for various lunar rocks. The reflectance results for the three rock chips shown in Figs. 2, 3, and 4 are given in Fig. 17. Clearly evident are a number of distinct absorption bands.

Adams and McCord [32] have presented diffuse reflectance for mineral separates for Apollo 12 basalt. They have demonstrated that the major absorption bands can be attributed to Fe^{2+} in pyroxene. All observed bands are attributed to electronic transitions in iron and titanium. Adams and McCord [37] have determined the relationship between the wavelength of the two major bands and the pyroxene composition. One band occurs

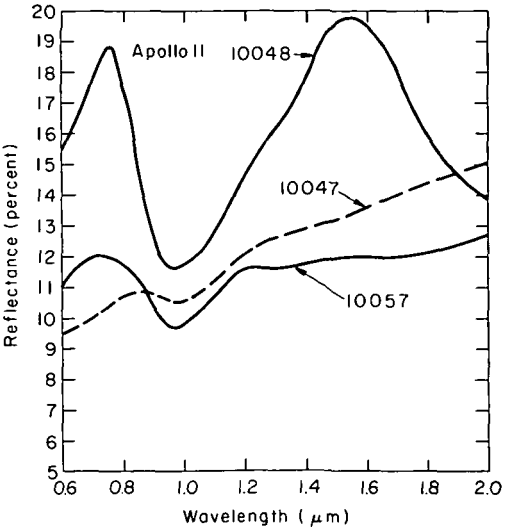

FIG. 17. Typical directional spectral reflectance of lunar rock chips—Apollo 11 mission.

between 0.9 and 1.0 μm and the second near 2.0 μm. The depth of the absorption bands is also a function of the average pyroxene composition and in the breccias, also of the glass content. The bands degrade from rocks to breccias to the fines material, and their depth or strength correlates with the percent increase of dark glass [14], a conclusion also reached by Conel

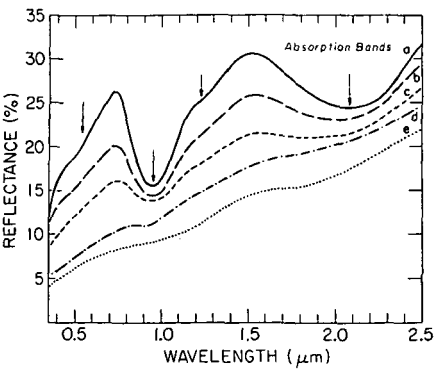

FIG. 18. Directional reflectance as a function of glass content—Apollo 12 mission. Symbols: a, 12063, 79 whole-rock powder; b, +20% glass; c, +55% glass; d, 12070, 111 surface fines; e, 12063, 79 whole-rock glass. (Reproduced from Adams and McCord [32].)

and Nash [33]. The effects of the addition of artificially made glass from the crystalline lunar rock is shown in Fig. 18.

Perry *et al.* [35, 36] have made reflectance measurements on lunar samples from Apollo 11, 12, 14, and 15. The spectra were obtained from polished specimens and over a wavelength range of 5–500 μm. The resulting spectra are very complex and are of more interest to the geophysicists than to the thermal engineer. No meaningful thermal property data can be obtained from these results.

b. Lunar Fines. Before we begin to discuss the directional reflectance properties of lunar fines it is desirable to reiterate the various parameters that affect the reflectance. It seems reasonable to assume that the bulk density or compaction of the material will affect the reflectance. The surface may become more compacted around equipment on the moon due to intentional packing or because of astronaut activities. Another reason for looking at the effect of density is that we still do not know what the exact density of the lunar surface is or how it varies over the lunar surface. Estimates [10] of the soil density from in-place measurements range from 800 to 2150 kg/m^3. However, it should be kept in mind that only the upper 10 mm or so actually affect the thermal radiation characteristics and the lower densities, therefore, could be reasonable estimates.

When a fines sample is prepared by simply pouring it into a container and carefully leveling the surface, the bulk density achieved depends on the distribution of particle size in the fines. With this procedure followed for the Apollo 14 and 15 fines, bulk densities of nearly 1000 kg/m^3 were obtained. Slightly higher values were obtained for the Apollo 11 and 12 samples. To achieve higher bulk densities [26] the fines were packed by use of a vibrating tool held on the sample holder edge. Initial smoothing and packing of the surface was achieved with a stainless steel spatula. Whether this procedure gives a surface texture close to that of the fines on the moon is open to question at this time.

A second parameter that affects the directional reflectance is the angle of illumination. The studies of our group [26, 29b, 38–40] are the only ones, to our knowledge, that have been made on lunar fines. As we discussed earlier, the heat flux to or from the lunar surface is greatly influenced by the angle of illumination that the solar energy makes with the lunar surface [6].

(i) *Spectral directional reflectance for fines.* The smooth curves for our data which are shown in the figures in this section are fit through data points taken at 0.02 μm intervals to 1.0 μm and 0.05 μm interval to 2.2 μm.

The spectral directional reflectance curves for fines from Apollo Missions 11, 12, 14, 15, and 16 are shown in Fig. 19. The results are for a bulk density of approximately 1600 kg/m^3 for each sample and for an angle of illumina-

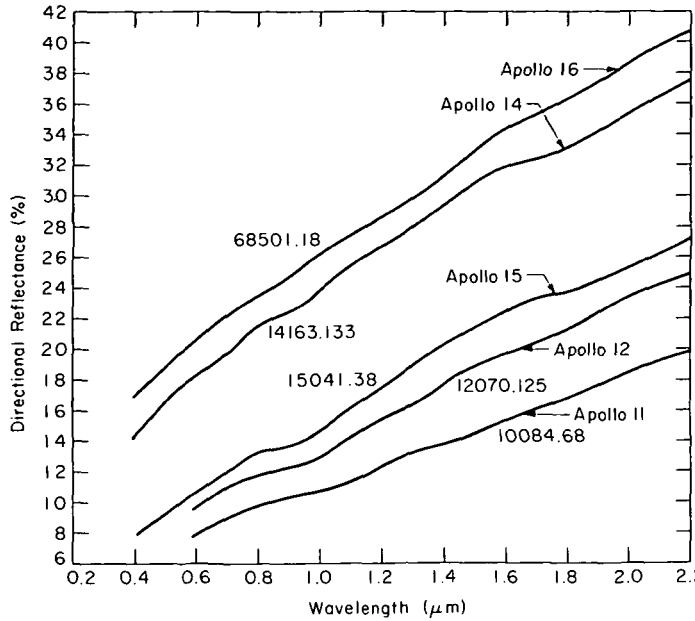

FIG. 19. Spectral directional reflectance of lunar fines from Apollo 11, 12, 14, 15, and 16 missions. Angle of illumination $\cong$ 10°, bulk density $\cong$ 1600 kg/m^3.

tion of approximately 10°. It is readily apparent by comparing Figs. 17 and 19 that the spectral results for fines are very different than for rocks. It is difficult sometimes to identify absorption bands in the fines data. The pyroxene band near 1.0 μm is apparent in the Apollo 12, 14, and 15 samples but undetectable by us in the Apollo 11 and 16 samples. The results of Adams and Jones [41] and Conel and Nash [33] show a single, very shallow absorption band centered at 0.95 μm for the Apollo 11 sample. Other investigators [27, 30], however, did not find any band features in this region of the spectrum.

Both the results of Birkebak and Dawson [40] and Adams and McCord [37] show an absorption band for the Apollo 14 sample centered at 0.93 μm and this band is due to pyroxene [37]. Also, a band is clearly evident at 1.8 μm.

The variation in reflectance from one Apollo sample to another is associated with its chemical composition and glass content [25, 32–34, 37, 41]. As the lunar fines become "lighter in color," an increase in reflectance, we find fewer opaque materials in the fines. Adams and McCord [37] have discussed the lighter appearances of Apollo 14 fines and have related it to the fines having lower overall iron and titanium content. The presence or

absence of the absorption bands are a function of the dark glass content and the crystal/glass ratio. The disappearance of the pyroxene band near 1 μm may be caused instead by extensive impact melting and shock alteration of the soil [32]. Material taken from the core tube samples or trench below 70 mm or so from the surface has a higher reflectance than the surface fines. The darkening of the surface material takes place due to meteorite impact-induced vitrification and by regional contamination by iron- and titanium-rich mare material.

The average composition of the Apollo 11, 12, 14, 15, and 16 fines are given in Table II [10, 43]. B. Glass [42] has reported that glass particles in the fines with low TiO_2 and FeO content ($<1\%$) and high Al_2O_3 ($\approx 33\%$) are colorless: as the TiO_2 and FeO content increases approximately 3 and 20%, respectively, and with a decrease in Al_2O_3 from 33 to 10%, the color of the glass changes from transparent pale green to yellow-green to yellow-brown to red and dark opaque red-brown.

The crystal-to-glass ratio is also an indication of the maturity [37] of the material: Apollo 11 fines were approximately 50% glass, Apollo 12, 20% glass, and Apollo 14, 40–75% glass [37].

Our Apollo 11, 12, and 15 samples can be classified as mare material, and Apollo 14 and 16 as lunar highlands material.

TABLE II

AVERAGE COMPOSITION OF LUNAR FINES

Compound	Lunar fines sample no. (% abundance)				
	10084[a]	12070[a]	14163[a]	15021[a]	68841[b]
SiO_2	41.86	45.91	47.17	46.56	45.08
TiO_2	7.56	2.81	1.79	1.75	0.59
Al_2O_3	13.55	12.50	17.22	13.73	26.49
FeO	15.94	16.40	10.35	15.21	5.65
MnO	0.21	0.22	0.14	0.20	0.07
MgO	7.82	10.00	9.37	10.37	6.27
CaO	12.08	10.43	10.95	10.54	15.30
Mg_2O	0.40	0.41	0.66	0.41	0.41
K_2O	0.13	0.25	0.58	0.20	0.11
P_2O_5	0.11	0.27	0.46	0.18	0.12
S	0.15	0.08	0.08	0.06	0.08
Cr_2O_3	0.32	0.43	0.22	—	—
	100.13	99.71	98.99	99.21	100.16

[a] "Apollo 15 Preliminary Science Report" [10].
[b] "Apollo 16 Lunar Sample Information Catalog" [43].

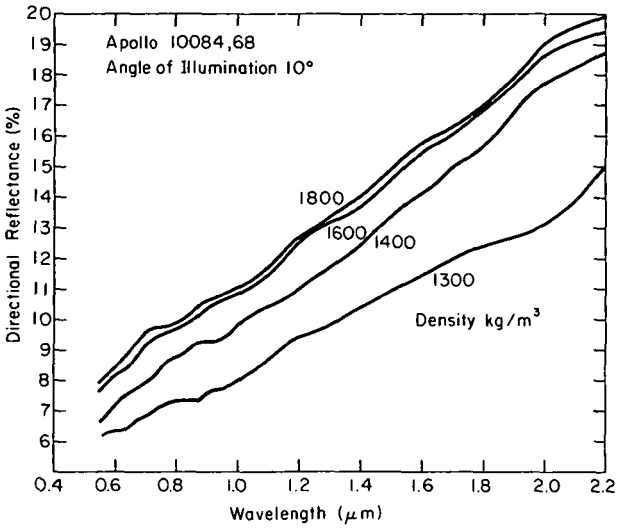

FIG. 20. Spectral directional reflectance as a function of bulk density—Apollo 11.

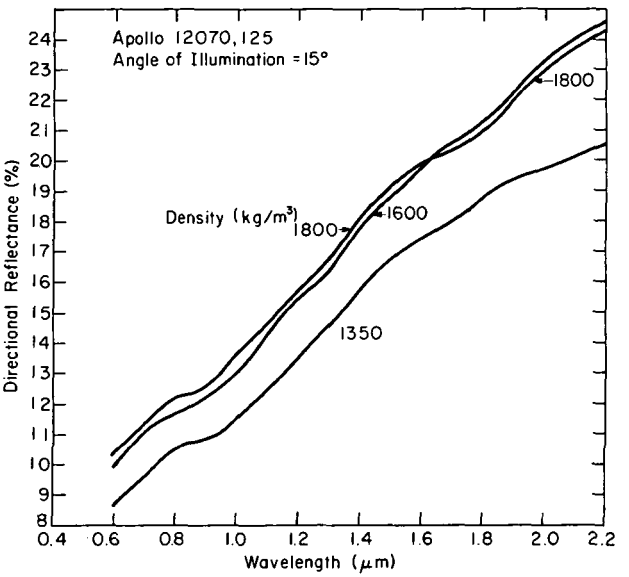

FIG. 21. Spectral directional reflectance as a function of bulk density—Apollo 12.

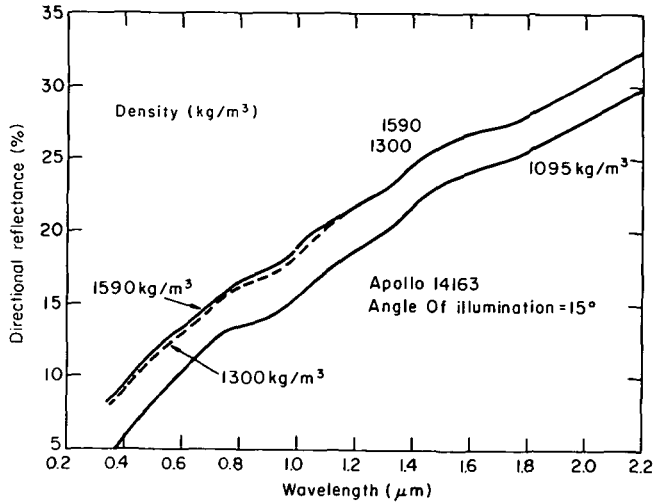

FIG. 22. Spectral directional reflectance as a function of bulk density—Apollo 14.

The spectral reflectances reported by other investigators show similar trends as ours. It is difficult to compare the results since they refer their reflectances to MgO samples and do not give the bulk density of their material.

The spectral directional reflectance of Apollo 11, 12, and 14 samples as a function of bulk density are presented in Figs. 20–22. In general, the reflectance increases with density for all wavelengths in the UV, visible, and near-IR regions. The Apollo 11 and 12 samples had very similar particle distributions for the smaller-size particles ($<10\ \mu$m) for a given size of particle. The Apollo 11 and 12 fines had essentially the same number of particles. This being the case, it is not surprising that their reflectances reach maximum values for the same density. The Apollo 14 fines have more particles [45] in this smaller particle range and their effect is seen in the results. Figure 22 shows that the Apollo 14 fines spectral reflectance reaches a maximum value for smaller bulk densities than the Apollo 11 and 12 samples, and this we attribute to the increased amount of small particles. As the surface becomes more compacted, that is, a greater number of particles per unit volume, the porosity decreases and hence fewer number of cavities to trap and absorb radiation are present, and as a result the reflectance increases. Further increase in density has no effect.

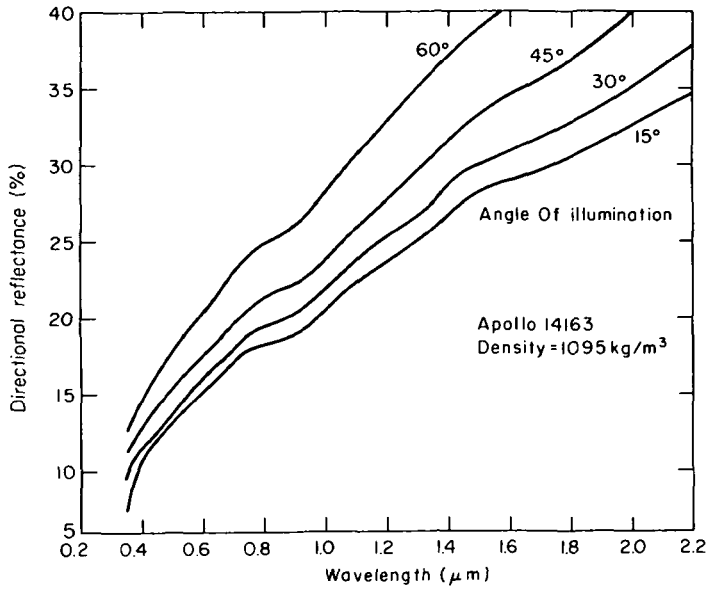

FIG. 23. Spectral directional reflectance as a function of angle of illumination—Apollo 14.

TABLE III

SOLAR ALBEDO FOR LUNAR FINES[a]

Sample density (kg/m³)	Angle of illumination (degrees)					
	10	15	20	30	45	60
Apollo 11, 10084						
1300	0.076	—	0.082	0.084	0.095	0.108
1400	0.087	—	0.095	0.102	0.113	0.132
1600	0.099	—	—	0.107	0.113	0.133
1800	0.101	—	0.102	0.108	0.116	0.132
Apollo 12, 12070						
1300	0.101	—	0.106	0.109	0.122	—
1600	0.119	—	0.114	0.115	0.136	—
1800	0.120	—	0.126	0.131	0.138	—
Apollo 14[b], 14163						
1095	—	0.18	—	0.194	0.216	0.250
1300	—	0.212	—	0.222	0.241	0.281
1590	—	0.213	—	0.221	0.262	0.297
Apollo 15, 15041						
1615	—	0.137	—	0.146	0.162	0.193

[a] Birkebak [48]. [b] Birkebak and Dawson [40].

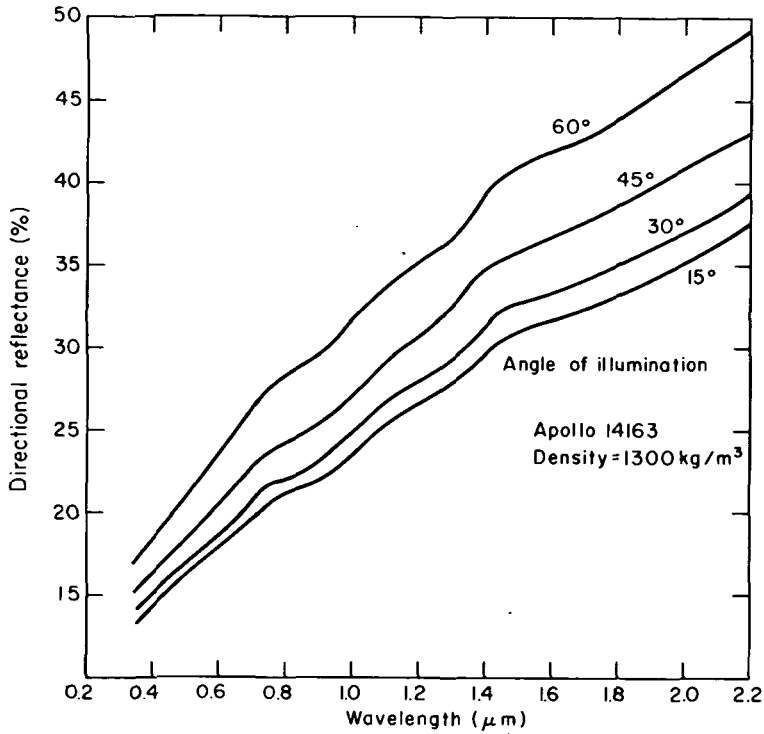

FIG. 24. Spectral directional reflectance as a function of angle of illumination—Apollo 14.

The effect of the angle of illumination is presented in Figs. 23–25 for the Apollo 14 fines [40]. The results for the other Apollo samples show the same features and trends. The reflectance increased with angle of illumination and this is what one would generally expect.

(ii) *Solar reflectance.* The solar reflectances were calculated from the spectral directional reflectance (Sect. C,2,i), spectral emittance results are to be discussed in the next section, and the spectral solar distribution of Johnson [44]. The solar reflectance (albedo) is defined as

$$\rho_s(\theta) = \int_{\lambda=0.3}^{\lambda=6.0} \rho(\lambda, \theta) S_\lambda \, d\lambda \Big/ \int_{\lambda=0.3}^{\lambda=6.0} S_\lambda d\lambda \qquad (9)$$

where $\rho(\lambda, \theta)$ is the spectral directional reflectance, θ is the angle of illumination, λ is the wavelength, and S_λ is the spectral value of the incident solar energy.

The solar reflectance for the Apollo 11, 12, 14, and 15 samples are pre-

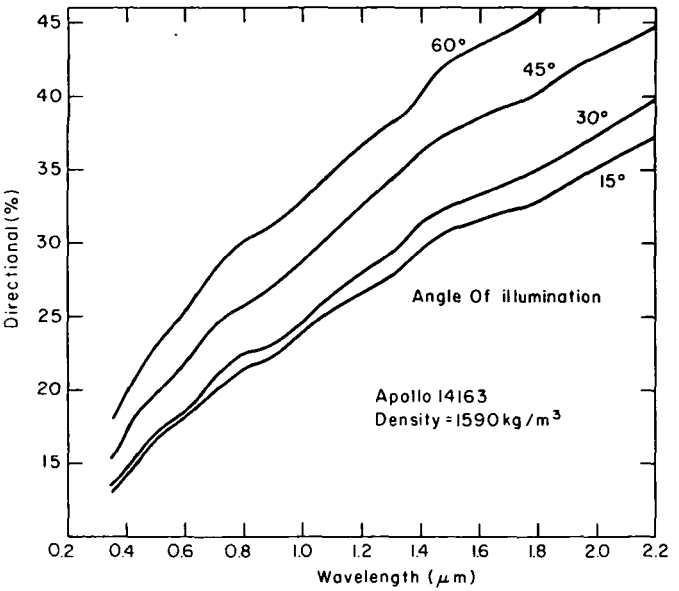

FIG. 25. Spectral directional reflectance as a function of angle of illumination—Apollo 14.

sented in Table III. Clearly evident is both a bulk density and angle of illumination effect. The change in solar reflectance with angle of illumination is characteristic of dielectric materials. The results for the Apollo 11, 12, and 14 samples were fitted to Eq. (10) and when $\theta = 90°$, the solar reflectance is 1:

$$\rho_s(\theta) = A + B\theta + C\theta^2 + D\theta^3 + E\theta^4 + F\theta^5 \qquad (10)$$

where the coefficients are given in Tables IV and V.

3. *Spectral Emittance*

The spectral emittance [24, 38] of sample 12070 as a function of bulk density for an angle of viewing of 15° is shown in Fig. 26. Each curve represents an average of 3 or more runs and were drawn through data points taken every 0.25 μm. The bandwidth for these measurements varied from 0.5 μm at 2.5 μm to 0.36 μm at 14.75 μm. The estimated error in these measurements is ±1%.

The sample surface temperature used in Eq. (8) was calculated from the measured sample temperature gradient, the temperature measured near the surface and from the known sample thickness and thermocouple locations. The temperature gradient in the test fines is similar to that during lunar

TABLE IV

COEFFICIENTS FOR DIRECTIONAL REFLECTANCE EQUATION[a]
$\rho_s(\theta) = A + B\theta + C\theta^2 + D\theta^3 + E\theta^4$

	Density (kg/m³)						
	Apollo 11, 10084				Apollo 12, 12070		
Coefficient	1300	1400	1600	1800	1300	1600	1800
$A \times 10$	0.7835	0.8896	1.005	1.0349	1.0098	1.192	1.20
$B \times 10^2$	−0.3452	−0.3304	−0.2674	−0.3472	−0.06783	−0.002479	−0.1041
$C \times 10^3$	0.3444	0.3405	0.2895	0.3316	0.09985	−0.002695	0.1411
$D \times 10^5$	−0.9604	−0.9379	−0.8452	−0.9191	−0.3515	−0.07244	−0.4614
$E \times 10^7$	0.8298	0.8059	0.7554	0.7960	0.4136	0.2184	0.4869

[a] Birkebak [48].

night. The surface temperature for all measurements was approximately 380°K, a temperature very near the maximum temperature experienced by the sample on the lunar surface [4–6].

The spectral emittance has a maximum of 0.995 at approximately 8.5 μm and a minimum of 0.71 at approximately 3.75 μm for a density of 1910 kg/m³. An absorption band is apparent and appears centered at 5.5 μm. The maximum emittance occurs at the so-called Christiansen frequency where the index of refraction of the surrounding medium and fines are equal and where internal scattering is a minimum.

The effects of density on emittance are very evident in Fig. 26. As the wavelength increases from 2.5 to 14 μm, the wavelength-to-particle-size

TABLE V

DIRECTIONAL REFLECTANCE COEFFICIENTS—APOLLO 14

Density (kg/m³)	$\rho_s(\theta) = A + B\theta + C\theta^2 + D\theta^3 + E\theta^4 + F\theta^5$					
	A	$B \times 10^2$	$C \times 10^3$	$D \times 10^4$	$E \times 10^6$	$F \times 10^8$
1095	0.18	0.052501	−0.11451	0.073283	−0.151057	0.106163
1300	0.212	0.045952	−0.092297	0.056681	−0.11649	0.084766
1590	0.213	0.3863	−0.51630	0.22219	−0.36203	0.20621

[a] Birkebak and Dawson [40].

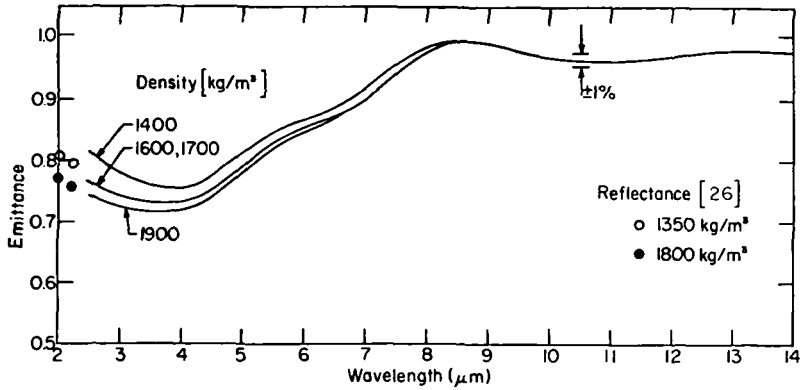

FIG. 26. Spectral emittance of lunar fines as a function of bulk density—Apollo 12.

ratio is such that beyond approximately 8 μm the density of the material is unimportant in the radiative transport process.

Comparison of 1 minus the reflectance results near 2 μm for various densities with the emittance data are good for the highest density but poor in agreement for the lowest density. This is not an unexpected result for the lower densities, since the fines have a tendency to settle due to vibration if kept for a period of time greater than several hours in the test apparatus.

The emittance results from Apollo 12, 14 [40], and 15 are compared in Fig. 27 for a density of 1600 kg/m³. All results have maximum emittance between 8 and 9 μm. The Apollo 14 maximum is at approximately 8.25 μm and Apollo 15 at approximately 8.4 μm. Logan *et al.* [46] have also measured the emittance for Apollo 14 sample 14259 over a smaller wavelength

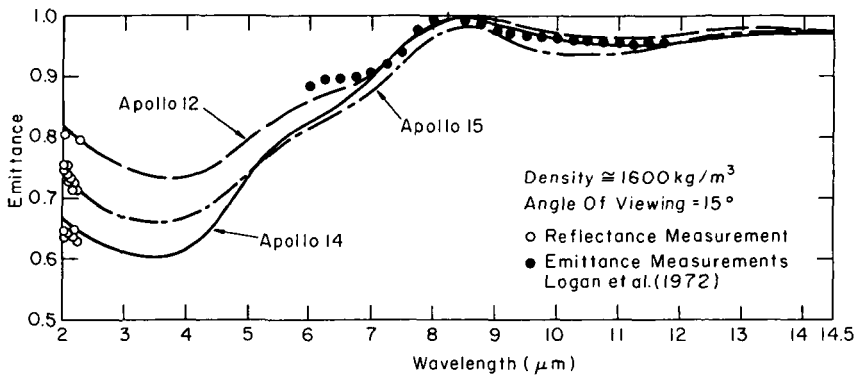

FIG. 27. Spectral emittance of Apollo 12, 14, and 15 lunar fines.

range than ours. They do not specify a bulk density for their measurement. They report a maximum emittance at 8.24 μm. Agreement of their results with ours is excellent. All samples have minimums at approximately 3.5–3.6 μm. Minimum value for Apollo 14, the lowest for all samples tested, is 0.60, for Apollo 12 the minimum is 0.73.

a. Total Emittance. The total normal emittance as a function of surface temperature was calculated using

$$\epsilon(\theta, T) = \int_0^\infty \epsilon(\lambda, \theta, T) i_B(\lambda, T)\, d\lambda \Big/ \int_0^\infty i_B(\lambda, T)\, d\lambda \qquad (11)$$

where $\epsilon(\lambda, \theta, T)$ is the directional spectral emittance, θ is the angle of viewing, T is the temperature of the sample, and $i_B(\lambda, T)$ is the Planckian radiance distribution.

The total emittance for Apollo 12 sample 12070 as a function of density and temperature is represented in Fig. 28. Also shown are total emittance data obtained directly from Apollo 11 sample 10084. Over the expected temperature range on the moon, 90–400°K, the total emittance varies from approximately 0.972 to 0.927. The equation representing the emittance as a function of temperature for a bulk density of 1910 kg/m^3 [38] is:

$$\epsilon(T) = 0.9843 - 0.2037 \times 10^3\, T + 0.1863 \times 10^{-5}\, T^2 - 0.6765 \times 10^{-8}\, T^3 + 0.6436 \times 10^{-11}\, T^4 \qquad (12)$$

where T is the absolute temperature in degrees Kelvin.

The Apollo 11 measurements are for a bulk density of 1600 kg/m^3. Over the limited temperature range of these results the total emittance varied between 0.89 and 0.98 $\pm$ 0.01. Many investigators who have studied the

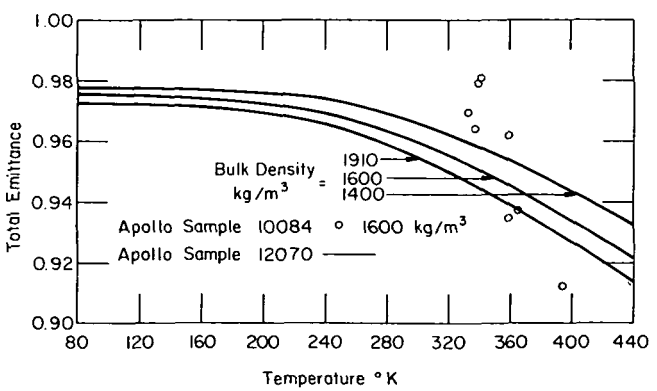

FIG. 28. Total emittance of Apollo 11 and 12 lunar fines.

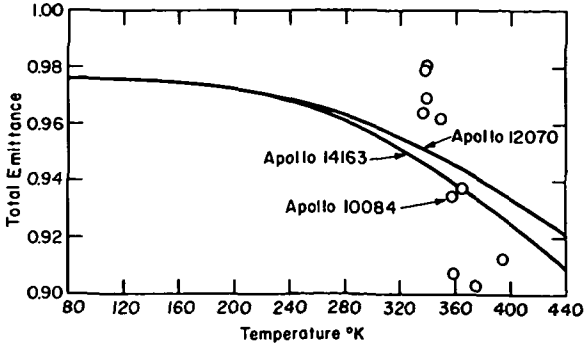

FIG. 29. Total emittance of Apollo 11, 12, and 14 lunar fines for a bulk density of 1600 kg/m³.

lunar surface temperature variation have assumed an emittance of unity, but from our results they can be as much as 9% high.

In Fig. 29 the total emittance of Apollo 11, 12, and 14 samples are compared for a bulk density of 1600 kg/m³. The Apollo 14 sample [47] shows the same general trend as the Apollo 12 results. At the lower temperature the results are identical but the total emittances are different for the higher temperatures. The spectral characteristics for the shorter wavelengths account for the difference in the total emittance of the two Apollo samples. Birkebak and Abdulkadir [47] have fitted a third-order polynomial to the Apollo 14 results and obtained

$$\epsilon(T) = 0.9696 + 0.9664 \times 10^{-4}\, T - 0.31674 \times 10^{-6}\, T^2 - 0.50691 \times 10^{-9}\, T^3 \qquad (13)$$

where T is in degrees Kelvin. At 90°K the total emittance is 0.976 and decreases to 0.925 at 400°K.

V. Summary

The thermal radiation properties of lunar fines and rocks have been reviewed. Only those papers which present results that have a direct bearing on heat transfer calculations have been considered. Two papers which were not reviewed but which deal with infrared measurements are by Bastin *et al.* [49] and Ade *et al.* [50]. Their results for the most part are for the far infrared region. The reviewed properties have been used by Cremers *et al.* [4–6] to calculate the temperature variations and heat flow on the lunar surface.

ACKNOWLEDGMENTS

I thank Ariono Abdulkadir, Mark and Todd Birkebak, and Charles Neville for their assistance in data reduction and equipment design. I also want to acknowledge my co-investigators Jim Dawson and Cliff Cremers for their support on our project. Our research was supported by the National Aeronautics and Space Administration under Contract NAS9-8098 and grants NGR 18-001-060 and 18-001-026.

NOMENCLATURE

A, B	Coefficients in Eq. (10)
B	Blackbody
B	Bond albedo
C	Coefficient in Eq. (10)
C_2	Second radiation constant
D	Coefficient in Eq. (10)
E	Coefficient in Eq. (10)
F	Coefficient in Eq. (10)
e	Radiant energy per unit area and time
i	Radiance (energy per unit time, projected area, and sterradian)
p	geometric albedo
q	Phase integral
R	Reference
S	Sample
S_λ	Spectral solar distribution
T	Temperature (°K)
V	Phase angle—angle between the sun, moon, and earth (degrees)
$\Delta( )$	Detector output
ϵ	Emittance
λ	Wavelength (micrometers)
θ	Angle of viewing (degrees)
Ψ	Angle of illumination (degrees)
ρ	Directional reflectance
$\Phi(V)$	Phase integral function (the amount of light reflected into unit solid angle around the direction toward the observer at phase angle V)
$\Delta\Omega$	Solid angle—sterradian

SUBSCRIPTS

b	Bidirectional reflectance
B	Blackbody
h	Hemispherical reflectance
i	Incident
r	Reflected
R	Reference
S	Sample
s	Solar
λ	Wavelength

REFERENCES

1. B. Hapke, *in* "Physics and Astronomy of the Moon" (Z. Kopal, ed.), 2nd Ed., Ch. 5. Academic Press, New York, 1971.
2. *Proc. Apollo 11 Lunar Sci. Conf., Science* **167** (1970).
3. "Apollo 12 Preliminary Science Report," *NASA Spec. Publ.* **NASA SP-235** (1970).
4. C. J. Cremers, R. C. Birkebak, and J. E. White, *AIAA J.* **9**, 1899 (1971).
5. C. J. Cremers, R. C. Birkebak, and J. E. White, *The Moon* **3**, 246 (1971).
6. C. J. Cremers, R. C. Birkebak, and J. E. White, *Int. J. Heat Mass Transfer* **15**, 1045 (1972).
7. J. A. Bastin and E. L. C. Bowell, *in* "Geology and Physics of the Moon" (G. Fielder, ed.), Ch. 11. Elsevier, Amsterdam, 1971.
8. T. Gold, M. J. Campbell, and B. T. O'Leary, Proc. *Apollo 11 Lunar Sci. Conf.; Geochim. Cosmochim. Acta*, Suppl. 1, **3**, 2149 (1970).
9. "Apollo 14 Preliminary Science Report," *NASA Spec. Publ.* **NASA SP-272** (1971).
10. "Apollo 15 Preliminary Science Report," *NASA Spec. Publ.* **NASA SP-289** (1972).
11. T. B. McCord and T. V. Johnson, *J. Geophys. Res.* **74**, 4395 (1969).
12. T. B. McCord and T. V. Johnson, *Science* **169**, 855 (1969).

13. T. B. McCord, M. P. Charette, T. V. Johnson, L. A. Lebofsky, and C. Pieters, *J. Geophys. Res.* **77**, 1349 (1972).
14. J. B. Adams and T. B. McCord, *Proc. Apollo 11 Lunar Sci. Conf.; Geochim. Cosmochim. Acta* Suppl. 1, **3**, 1934 (1970).
15. M. Rougier, *Ann. Observ. Strasbourg* **2**, 203 (1933).
16. B. W. Hapke, *J. Geophys. Res.* **68**, 4571 (1963).
17. A. V. Morozhenko and E. G. Yanovitskii, *Sov. Astron.—AJ* **15**, 134 (1971).
18. F H. Murcray, *J. Geophys. Res.* **70**, 4959 (1965).
19. F. H. Murcray, D. G. Murcray, and W. J. Williams, *J. Geophys. Res.* **75**, 2662 (1970).
20. J. W. Salisbury, R. K. Vincent, L. M. Logan, and G. R. Hunt, *J. Geophys. Res.* **75**, 2671 (1970).
21. J. E. Conel, cited in Salisbury *et al.* [20], p. 2676.
22. R. C. Birkebak, C. J. Cremers, and W. E. Lyons, *Rev. Sci. Instrum.* **42**, 1715 (1971).
23. R. C. Birkebak and C. J. Cremers, "Thermophysical Properties of Lunar Material." TR2, High Temp. and Therm. Radiat. Lab., Univ. of Kentucky, Lexington, 1971.
24. R. C. Birkebak, *J. Heat Transfer* **94**, 323 (1972)
25. B. W. Hapke, A. J. Cohen, W. A. Cassidy, and E. N. Wells, *Proc. Apollo 11 Lunar Sci. Conf.*; *Geochim. Cosmochim. Acta* Suppl. 1, **3**, 2199 (1970),
26. R. C. Birkebak, C. J. Cremers, and J. R. Dawson, *Proc. Lunar Sci Conf., 2nd*; *Geochim. Cosmochim. Acta* Suppl. 2, **3**, 2197 (1971).
27. T. Gold, B. T. O'Leary, and M. Campbell, *Proc. Lunar Sci. Conf., 2nd*; *Geochim. Cosmochim. Acta* Suppl. 2, **3**, 2173 (1971).
28. J. E. Geake, A. Dollfus, G. F. J. Garlick, W. Lamb, G. Walker, G. A. Steigmann, and C. Titulaer, *Proc. Apollo 11 Lunar Sci. Conf.*; *Geochim. Cosmochim. Acta* Suppl. 1, **3**, 2127 (1970).
29a. R. C. Birkebak, C. J. Cremers, and J. P. Dawson, *Science* **167**, 724 (1970).
29b. R. C. Birkebak, C. J. Cremers, and J. P. Dawson, *Proc. Apollo 11 Lunar Sci. Conf.*; *Geochim. Cosmochim. Acta* Suppl. 1, **3**, 1933 (1970).
30. B. T. O'Leary and F. Briggs, *J. Geophys. Res.* **75**, 6532 (1970).
31. B. Hapke, *Science* **159**, 77 (1968).
32. J. B. Adams and T. B. McCord, *Proc. Lunar Sci. Conf., 2nd*; *Geochim. Cosmochim. Acta* Suppl. 2, **3**, 2183 (1971).
33. J. E. Conel and D. B. Nash, *Proc. Apollo 11 Lunar Sci. Conf.*; *Geochim. Cosmochim. Acta* Suppl. 4, **3**, 2013 (1970).
34. D. B. Nash and J. E. Conel, *Proc. Lunar Sci. Conf., 2nd*; *Geochim. Cosmochim. Acta* Suppl. 2, **3**, 2235 (1971).
35. C. H. Perry, D. K. Agrawal, E. Anastassakis, R. P. Lowndes and N. E. Tornberg, *Proc. Lunar Sci. Conf., 3rd*; *Geochim. Cosmochim. Acta*, Suppl. 3, **3**, 3077 (1972).
36. C. H. Perry, D. K. Agrawal, E. Anastassakis, R. P. Lowndes, A. Rastogi, and N. E. Tornberg, *The Moon* **4**, 58 (1972).
37. J. B. Adams and T. B. McCord, *Rev. Abstr., Lunar Sci. Conf., 3rd* Lunar Sci. Inst., Houston, Contrib. No. 88 (1972).
38. R. C. Birkebak, *The Moon* **4**, 128 (1972).
39. R. C. Birkebak and J. P. Dawson, *Rev. Abstr., Lunar Sci. Conf., 3rd* Lunar Sci. Inst., Houston, Contrib. No. 88 (1972).
40. R. C. Birkebak and J. P. Dawson, *The Moon* **5**, 157 (1972).
41. J. B. Adams and R. L. Jones, *Science* **167**, 737 (1970).
42. B. Glass, *Rev. Abstr., Lunar Sci. Conf., 3rd* Lunar Sci. Inst., Houston, Contrib. No. 88 (1972).

43. "Apollo 16, Lunar Sample Information Catalog," Lunar Receiving Lab., NASA, MSC 03210 (1972).
44. F. S. Johnson, *J. Meteorol.* **11**, 431 (1954).
45. T. Gold, E. Bilson, and M. Yerbury, *Rev. Abstr., Lunar Sci. Conf., 3rd* Lunar Sci. Inst., Houston, Contrib. No. 88 (1972).
46. L. M. Logan, G. R. Hunt, S. R. Bolsamo, and J. W. Salisbury, *Rev. Abstr., Lunar Sci. Conf., 3rd* Lunar Sci. Inst., Houston, Contrib. No. 88 (1972).
47. R. C. Birkebak and A. Abdulkadir, *J. Geophys. Res.* 77, 1340 (1972).
48. R. C. Birkebak, *AIAA J.* **10**, 1064 (1972).
49. J. A. Bastin, P. E. Clegg, and G. Fielder, *Proc. Apollo 11 Lunar Sci. Conf.*; *Geochim. Cosmochim. Acta* Suppl. 1, **3**, 1987 (1970).
50. P. A. Ade, J. A. Bastin, A. C. Marston, S. J. Pandya, and E. Puplett, *Proc. Lunar Sci. Conf., 2nd*; *Geochim. Cosmochim. Acta* Suppl. 2, **3**, 22 (1971).

Page intentionally left blank

Reprinted from:
ADVANCES IN HEAT TRANSFER, VOL. 10
© 1974
ACADEMIC PRESS, INC.

Thermophysical Properties of Lunar Media: Part II

HEAT TRANSFER WITHIN THE LUNAR SURFACE LAYER

CLIFFORD J. CREMERS

Department of Mechanical Engineering, University of Kentucky, Lexington, Kentucky

I. Introduction 39
II. Thermal Conductivity 42
A. Lunar Rocks 42
B. Lunar Fines 45
III. Specific Heat 59
A. Lunar Rocks 59
B. Lunar Fines 63
IV. Thermal Diffusivity 64
A. Lunar Rocks 64
B. Lunar Fines 68
V. Thermal Parameter 70
VI. Heat Transfer in the Lunar Surface Layer 72
VII. Reference Values of Thermophysical Properties 79
Nomenclature 80
References 80

I. Introduction

Heat transfer within the lunar surface layer depends on several thermophysical properties of the lunar regolith, that is, the material making up the surface layer. These include the thermal conductivity, specific heat, thermal diffusivity, and thermal parameter.

The thermal conductivity is a transport property defined by the Fourier law of heat conduction. It relates the flow of heat in an opaque quiescent medium to the temperature gradients therein. The specific heat relates

internal energy change to temperature change of a medium. Together, the thermal conductivity and specific heat are key transport properties for energy transfer calculations in solid media. Once they are known, the energy equation, which is just a statement of the first law of thermodynamics, can be solved for the temperature field in a medium with known boundary conditions. This along with Fourier's law permits calculation of local heat fluxes.

The other two properties mentioned in the first paragraph of this section are defined in terms of the thermal conductivity, specific heat, and density. The thermal diffusivity is given by $\alpha = k/\rho c$ and the thermal parameter is given by $\gamma = (k\rho c)^{-1/2}$. Both of these derived properties are useful in the solution of the transient energy equation, and their magnitudes give insight to the thermophysical nature of the medium in question. This has been particularly true in the study of energy transfer on the moon.

The thermal parameter is of particular historical interest in lunar research as it appears as a parameter in constant property solutions of the transient energy equation describing heat transfer on the moon. Such solutions formerly were compared with remote earth-based measurements of lunar temperatures inferred from infrared and microwave radiation measurements. The value of the thermal parameter which gave best agreement with measurement was then used as a clue as to the constitution of the lunar surface layer.

The nature of the moon's surface had been open to question until fairly recently. Certainly, telescopic observations had shown that the surface was composed of dielectric material, probably similar to terrestrial rocks of one sort or another. However, the first breakthrough did not come until 1929 when Epstein [1] analyzed the infrared eclipse data of Pettit and Nicholson [2]. The conclusion drawn from the low inferred value of γ was that the moon's surface was similar in character to pumice stone.

Pettit [3], using an improved technique, again measured the infrared radiation from the moon during an eclipse. Wesselink [4] analyzed this later data and obtained about the same value for γ as Epstein had. However, he showed that the resultant inferred thermal conductivity was about 12 times less than that measured for pumice stone. He compared his results with those obtained from vacuum samples of finely divided powders and concluded that the moon must be covered with a layer, probably thin, of powdered rock.

Subsequent refinements on Wesselink's model (e.g., Jaeger [5]) showed that the measured radiation could be best explained by a model which has a thin (several millimeters) layer of dust over a solid rock substrate. This idea has been popular until fairly recently.

Beginning in the early 1960's significant observations were made at

millimeter and centimeter wavelengths. Much of this work is summarized by Krotikov and Troitsky [6]. Assuming constant properties, these measurements indicated a homogeneous, highly insulating surface for a depth of several meters with a thermal parameter on the order of one-third that indicated by infrared measurements. These apparent contradictions in the properties of the lunar surface layer led to contradictory and disturbing conclusions when interpreted in the light of constant properties.

Linsky [7], in a review of possible models of the lunar surface, interprets the problem in the following way. The apparent contradiction can be explained if one or both sets of observations has been interpreted incorrectly. Alternatively, there must be a mechanism whereby the lunar material can exhibit insulating properties (large thermal parameter) at the surface during lunar nighttime for the infrared measurements. At the same time it must exhibit a significantly smaller thermal parameter at depths on the order of a meter where the observed long-wave radiation originates.

At nighttime, then, near the surface the product (kpc) must be considerably smaller than it is farther below the surface. At the same time, however, the long-wave data apparently do not allow the surface material to exhibit different thermal properties on the average during a lunar day than the material below it. The conclusion is that the thermal conductivity and specific heat both increase with temperature. The reasoning that led to these conclusions, based on data acquired at a distance of almost 4×10^5 km, is ingenious, and the later landings on the moon with the subsequent return and analysis of the samples showed how correct the conclusions were.

There have been a number of soft landings on the moon in the past several years including five unmanned Surveyor flights and five manned Apollo flights by the United States, and several unmanned Luna flights by the Soviet Union. Only two of these missions, Apollo 15 and Apollo 16, included provision for on-site measurement of surface layer thermophysical properties and then only the thermal conductivity. Unfortunately, a mishap caused the destruction of the Apollo 16 experiment. The only other flight which included such experiments was Apollo 13 which was aborted before a landing could take place. Consequently, there is only one set of on-site data available at this time.[1]

The successful landings on the moon of the Apollo flights, along with the return of samples of the surface material, have permitted the measurement of the thermophysical properties necessary for heat transfer calculations. These explorations have also proved what was previously hypothesized—

[1] Subsequent to the preparation of this manuscript, the Apollo 17 mission was successfully carried out. Thermal conductivity and heat flow data were telemetered to earth and are now being analyzed.

that the lunar surface is covered to a depth of several meters or more, at least in the mare regions, with a layer of fine particulate soil (or *fines* as it has been called). There is a hard substratum below these fines and there are many rocks and sometimes boulders scattered about as well. However, these occur randomly and may be considered perturbations in the porous powdery surface layer.

Heat transfer within the surface layer will depend primarily on the properties of the fines. Consequently, a great deal of effort has gone into the measurement of the properties of this material from returned samples, with somewhat less effort being expended on the rocks and rock chips. In what follows, reference will be made to these samples by sample number as cataloged by the Manned Spacecraft Center, NASA, Houston, Texas. For further information on the location of the samples on the moon, their collection and handling, the interested reader is referred to references [8–10] as well as to the Office of the Curator, NASA, Houston.

As only a minute portion of the moon's surface has been visited so far, there is little justification for rejecting all of the previous models of lunar simulation. Some of these may well apply in areas not yet sampled. For that reason results of property measurements on simulated lunar materials will be presented where appropriate as well as measurements made on the actual samples themselves.

II. Thermal Conductivity

A. Lunar Rocks

There had not been much work of note regarding the thermal conductivity of lunar rocks prior to the return of the Apollo samples. By the time scientists became concerned with lunar heat transfer, it had already been established that the moon was apparently covered with a layer of dust or fines. Wechsler and Glaser [11] reviewed conductivity measurements of a number of candidate materials, including rocks. They also made measurements of both conductivity and specific heat on some of the more promising materials. Some of their results are shown in Table I. Note that in all cases the thermal conductivity increases with temperature. The conductivities reported by Wechsler and Glaser were obtained using the line heat-probe technique which is a variation of the line heat-source technique to be described later in the discussion concerning the lunar fines. For this method, a hole slightly larger than the probe is drilled in the rock to be tested and the probe is then inserted. Good thermal contact is insured by using mercury and Wood's metal as contact agents.

The thermal conductivity of a synthetic lunar rock and a number of

TABLE I

THERMAL PROPERTIES OF SELECTED ROCKS[a]

Material	Specific heat[b] (J/kg-°K)		Thermal conductivity (W/m-°K)		
	293–498°K	293–823°K	293°K	493°K	693°K
Semiwelded tuff[c]	837	1005	0.54	0.54	0.63
Obsidian	879	1005	0.96	1.05	1.13
Basalt[c]	879	963	1.25	1.47	1.68
Altered rhyolite	879	963	0.71	0.80	0.88
Serpentine	1088	1256	3.00	—	—
Granodiorite[c]	879	1005	1.72	1.76	1.77

[a] From Wechsler and Glaser [11].
[b] Average values within given temperature range.
[c] Thermal conductivity, Univ. of Calif. data, Stephens [12].

terrestrial igneous rocks at temperatures near melting is given by Murase and McBirney [13]. Their results all fall between 4.2 and 42 W/m-°K. This is on the order of a factor of ten or more larger than the conductivities of the solid materials.

There have been only a few studies of the thermal conductivity of the returned lunar rocks themselves. These have all been from the Apollo 11 mission and only one study involved a direct measurement, an indifferent one at that, which serves to indicate the difficulty in this kind of experiment.

Warren *et al.* [14] made a rough determination of the thermal conductivity of lunar rock 10046. This measurement was really a by-product of their specific heat measurement (discussed on p. 62). At about 4°K, they measured the temperature difference across the rock, assumed a linear temperature gradient, and calculated a thermal conductivity of 1.05×10^{-3} W/m-°K which is extremely low for rock of any type. However, it is well known that phonon conduction decreases significantly with temperature for rocks at temperatures below 100–200°K, and so these results must stand, at least until more detailed measurements are made at such low temperatures.

There are three other sets of rock thermal conductivities and these are derived from measured thermal diffusivities and specific heats using the relation $k = \alpha\rho c$. Horai *et al.* [15] measured the thermal diffusivity of four different rocks of two different types (these measurements are discussed in detail in Sect. IV, A). The samples analyzed were 10020 and 10057 (fine-grained vesicular crystalline igneous rocks—type A), along with 10046 and 10065 (breccias—type C). The specific heat was calculated as a function of temperature from the known mineral composition for these two classes of rocks. The results are shown in Fig. 1.

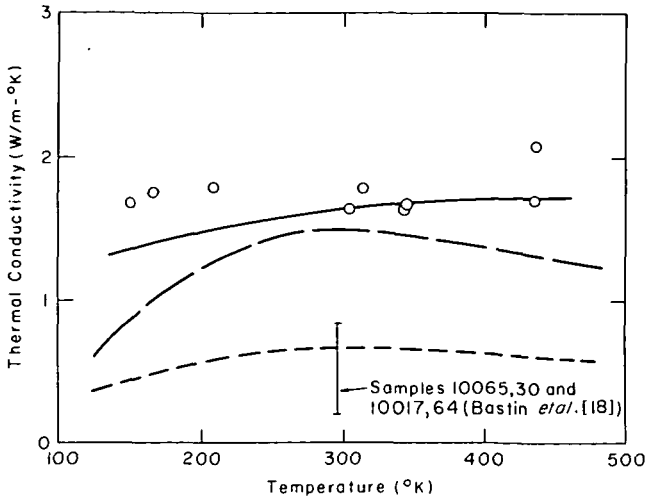

FIG. 1. Thermal conductivity of lunar and terrestrial rocks: —, terrestrial basalt [12]; – –, samples 10020, 10057 [15]; - - -, samples 10046, 10065 [15]; O, sample 10057 [16].

A second set of conductivities was derived by Robie and Hemingway [16] from the diffusivity data of Horai *et al.* [15] for rock 10057, only using their own measured specific heats for the same rock. These results are given in Table II and they are also displayed in Fig. 1. It is significant to note the differences between the results of Horai *et al.* [15] and Robie and Heming-

TABLE II

CALCULATED THERMAL CONDUCTIVITY OF LUNAR BASALT (10057)[a]

Temp. (°K)	Measured diffusivity[b] (m^2/sec)	Measured specific heat[c] (J/kg-°K)	Calculated thermal conductivity (W/m-°K)
149	11.94×10^{-7}	4.148×10^2	1.683
166	11.03	4.680	1.753
208	9.06	5.802	1.787
304	6.44	7.531	1.649
313	6.86	7.660	1.787
344	6.06	8.079	1.666
345	5.91	8.096	1.628
435	5.37	9.335	1.704
436	6.55	9.347	2.080

[a] From Robie and Hemingway [16]. [b] Horai *et al.* [15]. [c] Robie *et al.* [17].

way [16]. Whereas the former show that the conductivity of this particular basaltic rock has a significant dependence on temperature, the latter show that it has very little dependence on temperature. Also shown for comparison is a conductivity curve obtained for terrestrial basalt by Stephens [12]. The fairly good agreement between the latter two sets of data indicates that perhaps the specific heat assumption of Horai *et al.* [15] leaves something to be desired.

Bastin *et al.* [18] used a method of measurement whereby a thermal step function was applied to the sample by a straight electrically heated wire. Then from an independent measurement of the specific heat the conductivity was again derived as above. No details were given as to the sample temperature and so presumably it was at room temperature conditions. They obtained a range of conductivities of 0.209–0.837 W/m-°K for the type A rock (no identification given) and breccia (10065). This result is also shown in Fig. 1.

In summary there is not much that can be said concerning the thermal conductivity of lunar rock. Perhaps the best values one can use for heat transfer calculations involving this material are those for corresponding terrestrial types of rocks. An excellent summary of the available data for these is given in Wechsler and Glaser [11].

B. LUNAR FINES

It was mentioned previously that there has long been a suspicion that the lunar surface layer was composed primarily of powdered rock, soil or fines as it has lately been called. This has been found to indeed be the case at all the manned and unmanned mission sites visited to date. In fact, orbital photography gives the indication that this particulate layer exists almost universally on the moon. Consequently, considerably more effort has been expended on determining the thermophysical properties of this material than has been expended on the rocks. This is true for both simulated and actual lunar fines. In what follows, then, it will be frequently possible to make direct comparisons between the simulated lunar specimens and the actual samples.

The measurement of the thermal conductivity of a particulate medium such as the lunar fines is not straightforward. Any porous material with an internal temperature gradient will transfer heat through a complicated interaction between phonon conduction through the particles and their contact surfaces plus radiation which can be scattered in the voids and transmitted or absorbed and reemitted by the solid material. Under lunar conditions, of course, there is no problem caused by gaseous conduction or convection because of the extremely low pressures (on the order of 10^{-12} Torr).

One has, then, a heat transfer problem involving both conduction and radiation. If the heat flux is to be considered as an entity rather than as a two-component flux, then Fourier's law may be used, provided that it is recognized that the thermal conductivity so defined is only an "effective" one rather than a basic property of the material.

A number of authors, beginning with Wesselink [4] and including Watson [19], Clegg *et al.* [20], and Wildey [21], have shown that consideration of a radiative component of the heat flux leads to a cubic temperature dependence of the thermal conductivity. The derivation due to Clegg *et al.* [20] is conceptually the most satisfying and its essential arguments follow.

The net heat flux is assumed to be the sum of phonon conduction plus radiative transport, or $Q = Q_c + Q_r$. The following assumptions are then made:

(1) the surface layer is flat, homogeneous, deep, and in local thermodynamic equilibrium;

(2) scattering of thermal radiation within the surface layer is negligible;

(3) the medium is optically thick so that the Rosseland mean absorption coefficient may be used; and

(4) the optical depth (inverse absorption coefficient) is small compared with $T(\partial T/\partial x)^{-1}$ where T is the temperature at a depth x below the surface.

The radiative transfer equation for the net flux change in the direction s is

$$dI_\nu/ds = \kappa_\nu'(B_\nu - J_\nu) \tag{1}$$

where J_ν is the intensity of radiation of frequency ν and B_ν is the Planck blackbody function. κ_ν' is the given from the optical absorption coefficient by $\kappa_\nu' = \kappa_\nu[1 - \exp(-h\nu/kT)]$. s is the position coordinate in the direction of net flux. If Eq. (1) is solved for J_ν by the variable coefficient method, there results for the intensity of flux at any point O

$$J_\nu(O) = \int_0^\infty B_\nu(-\tau_\nu) \exp(-\tau_\nu)\, d\tau_\nu \tag{2}$$

where the point in question is taken as the origin of coordinates and where $d\tau_\nu = \kappa_\nu'\, ds$. Now $B_\nu(-\tau_\nu)$ can be expanded in a Taylor series about the origin under the condition that the point is much farther from the surface than $1/\kappa_\nu'$. Then if a Cartesian coordinate system is introduced so that the direction x is directed vertically down from the surface, the substitution $d\tau_\nu = \kappa_\nu'\, dx/\cos\theta$ may be made. Here θ is the angle between the direction of the radiation and the x axis. One then finds that the total downward

radiant energy flux is

$$2\pi \int_0^{\pi} J_\nu \cos\theta \sin\theta \, d\theta = -\frac{4\pi}{\kappa_\nu'} \frac{\partial B_\nu}{\partial x} \tag{3}$$

at least to a second order approximation. The total downward radiant flux taken over all frequencies is then given by

$$Q_r = -\frac{4\pi}{3} \int_0^{\infty} \frac{1}{\kappa_\nu'} \frac{\partial B_\nu}{\partial x} d\nu$$

$$= -\frac{4\pi}{3} \frac{\partial T}{\partial z} \int_0^{\infty} \frac{1}{\kappa_\nu'} \frac{\partial B_\nu}{\partial T} d\nu \tag{4}$$

and if the Rosseland mean absorption coefficient is introduced so that

$$\int_0^{\infty} \frac{1}{\kappa_\nu'} \frac{\partial B_\nu}{\partial T} d\nu = \frac{1}{\bar{\kappa}'} \int_0^{\infty} \frac{\partial B_\nu}{\partial T} d\nu \tag{5}$$

and if

$$\int_0^{\infty} \frac{\partial B_\nu}{\partial T} d\nu = \frac{\partial}{\partial T} \int_0^{\infty} B_\nu \, d\nu = \frac{\partial}{\partial T} \left(\frac{\sigma T^4}{\pi} \right) \tag{6}$$

then there results

$$Q_r = -\frac{16}{3} \frac{\sigma T^3}{\bar{\kappa}'(T)} \frac{\partial T}{\partial x} \tag{7}$$

The total heat flux, then, due to both conduction and radiation may be written

$$Q = -k_c \frac{\partial T}{\partial x} - \frac{16}{3} \frac{\sigma T^3}{\bar{\kappa}'(T)} \frac{\partial T}{\partial x} = -[k_c + k_r] \frac{\partial T}{\partial x} \tag{8}$$

where

$$k_r = \frac{16}{3} \frac{\sigma T^3}{\bar{\kappa}'(T)} \tag{9}$$

is the radiative component of the effective thermal conductivity and k_c is the solid or phonon conductivity.

In practice, $\bar{\kappa}'(T)$ does not vary significantly with temperature, nor does k_c, at least when compared with k_r. Consequently, this elementary theory predicts an effective conductivity of the form

$$k = A + BT^3 \tag{10}$$

As will be seen in the following, this expression fits the thermal conductivity data fairly well. In addition, Linsky [7] and Winter and Saari [48] in their

developments of lunar surface models showed that the assumption of thermal behavior implied by Eq. (10) led to good agreement between temperatures predicted by the models and those obtained from remote microwave or infrared radiation measurements.

It is obvious from Eq. (10) and the prior discussion that ambient pressure, temperature, and sample porosity are important parameters affecting the thermal conductivity of porous materials. As the porosity of a particulate medium is a function of the density of the material, given that the particle sizes and shapes are fixed by other considerations, the final constraints on the measurement of this property of the lunar fines are straightforward. An experiment to measure the thermal conductivity of the lunar fines or any powdered material in vacuum must provide a low pressure to suppress gaseous effects, and provision must also be made for control of sample density and ambient temperature for proper determination of the thermal conductivity over the range of lunar temperatures and surface layer densities.

There are many methods that have been developed to measure the thermal conductivity of a solid substance. Only a limited number of these are applicable to powdered low-conductivity materials. Watson [19] and Bastin *et al.* [18] used radiation techniques whereby the specimen sits on a heated surface for which the temperature can be measured as a function of time. A radiation detector monitors the flux from the free surface of the sample as a function of time after a step in the heating is applied. The response is a function of the heat capacity as well as the thermal conductivity and so the method is really a variation of a common method of thermal diffusivity measurement. Excellent reviews of early efforts for measuring conductivities of evacuated powder samples are given by Wechsler and Glaser [11], Wechsler and Glaser [22], Wechsler and Kritz [23], and Wechsler and Simon [24]. Most of the methods used required fairly large amounts of material to be tested.

Sample size was an important consideration in planning the experiment for the lunar samples themselves because only a few grams of lunar fines were to be made available. Using expected densities, this meant only about 2 cm^3 of material. After a great deal of experimenting, it was decided that the line heat-source technique was the best available method. The theoretical treatment of this approach is given by Carslaw and Jaeger [25] and the errors involved in its application are given by Blackwell [26]. Variations of the method have been used previously to determine the thermal conductivities of simulated lunar samples under vacuum, e.g., Wechsler and Glaser [11, 22] and Fountain and West [27], and also of other poor conductors, e.g., Mulligan [28]. The test cell and method used are described in detail by Cremers [29].

Briefly, the application of this method as used for the lunar sample analysis requires that a long (length-to-diameter ratio greater than 30) line heat-source be embedded in the material to be tested. For such a source in an infinite medium, it can be shown that after an initial period during which the probe heat capacity is dominant, the temperature change at any point in the medium over a time period from t_1 to t_2 is given by

$$T_2 - T_1 = q/(4\pi k) \ln(t_2/t_1) \tag{11}$$

Here q is the heat-source strength and k is the thermal conductivity of the medium. Note that k must be considered constant over the temperature range $T_2 - T_1$ under consideration.

Equation (11) is the usual working equation for the line heat-source method. It is apparent that if the conditions for the model are met in the experiment, a plot of temperature versus the logarithm of time will result in a straight line, the slope of which is $q/4\pi k$. The measurement of q and the slope of the curve then yields the thermal conductivity k.

The lunar samples which were made available for analysis were limited in volume so that it became imperative to measure the temperature as close to the source as possible to minimize deviations from the infinite medium assumption. For this reason the line source itself, a 36 AWG (0.127-mm diam.) Chromel-A wire, was calibrated as a resistance thermometer. Then with the wire in place in the sample the voltage change over about 22 mm of the wire was monitored during heating along with the voltage itself and the current flow. The current through the wire was controlled by a constant-current power supply which supplied a current constant to within four significant figures. The voltage change during a run was 0.25% at the maximum, and so the heat generation was constant to within this value as well. Axial heat conduction loss was minimized by providing an extra 20 mm of heating wire beyond the voltage taps and outside of the sample.

The test cell was constructed of Teflon and held about 5 g of the lunar fines at a density of 1100 kg/m^3. The size of the sample when in the cell was about 25 × 13 × 13 mm. The lowest density of the fines, that achieved by light pouring, was about 1100 kg/m^3 for the Apollo 14 fines and about 1300 kg/m^3 for the Apollo 11 and Apollo 12 fines. To obtain greater densities the cell was vibrated with a Vibrotool etching tool to cause uniform settling and packing.

The vacuum chamber was of stainless steel and was approximately 0.3 m high. The chamber was pumped with a Welsh Turbomolecular pump to provide a pressure on the order of 10^{-6} Torr. It will be seen later that this is well below the pressure at which gaseous effects are apparent. Electrical feedthroughs were provided for power and for temperature control and sensing.

TABLE III

VACUUM THERMAL CONDUCTIVITY OF TERRESTRIAL MATERIALS SIMILAR TO LUNAR FINES

Material	Density (kg/m³)	Temp. (°K)	Thermal conductivity (W/m-°K)
Olivine[a]	n.a.[d]	295	6.0×10^{-3}
Olivine[b]	1070	298	4.56
Basalt[a]	1270	283	2.0
Basalt[c]	1490	283	2.6
Chondrite[a]	n.a.	295	4.1
Tektite[a]	n.a.	281	2.3
Glass beads[b]	1380–1680	298	1.65
Glass beads[a]	1460	298	2.5
Pumice[a]	802	296	1.4
Granite[a]	1130	297	2.1
Hornblende[b]	1100–1500	298	3.45

[a] Wechsler and Glaser [11]. [b] Watson [19]. [c] Bernett *et al.* [30]. [d] Data not available.

An inner stainless-steel chamber of double-walled construction was used for ambient temperature control. A heating tape wrapped about the outer wall provided higher than room temperatures, and liquid nitrogen or expanding freon passed through the jacket provided low temperatures. A thermistor attached to the chamber actuated the heater for temperature control, and a thermocouple immersed in the sample indicated the sample temperature. Data were taken and processed by a small laboratory computer.

Measurements of the thermal conductivity of simulated lunar fines are summarized in Table III. In many cases the numbers given represent averages of a number of published data values for roughly similar conditions. Details as to particle-size range, method of packing, and method of measurement, as well as further data may be obtained from the references cited in Table III.

Wechsler and Glaser [11] in their study of postulated lunar materials reported measurements of the thermal conductivity of glass beads and powdered rocks. The latter consisted of basalt, chondrite, tektite, olivine, pumice, and granite. The densities are not all the same and presumably they represent values for the material as settled after a slight disturbance. Watson [19] did a study of heat transfer on the moon and as part of this he measured the thermal conductivity of glass microbeads, both crushed and

uncrushed, crushed quartz, olivine, and hornblende. Bernett *et al.* [30] reported measurements on basalt at several densities.

Note that the thermal conductivity values in Table III are all given for temperatures just below 300°K. As the temperatures at the lunar equator vary from about 100°K to 400°K, the values given in Table III are of only limited use in making calculations involving simulated lunar models.

The temperature dependencies of the thermal conductivity of glass beads, olivine, and basalt have been established by several authors. These terrestrial materials were suspected to be close in nature to the lunar fines. The Apollo samples have all had significant amounts of glass in them (up to about 50% for the Apollo 11 fines), and the lunar rock, which in powdered form makes up a great deal of the remainder of the fines, is similar to terrestrial basalt. Data of Watson [19] and Wechsler and Simon [24] for glass microbeads are shown as least-squares curves in Fig. 2. In both cases, the plots represent least-squares curves of the form of Eq. (10) fitted to the experimental data. Curves for crushed quartz are also shown for comparison. Similar data on olivine from Watson [19] and basalt from Wechsler and Simon [24] and Fountain and West [27] are shown in Fig. 3. The coefficients of Eq. (10) used in presenting the above data are given in Table IV. Bernett *et al.* [30] also measured the conductivity of olivine basalt as a function of temperature over the approximate range 200–350°K.

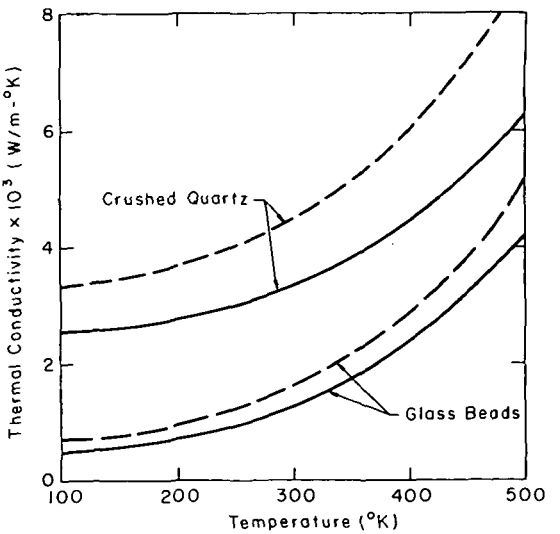

FIG. 2. Thermal conductivity of glass beads and crushed quartz. —— Wechsler and Simon [24], - - - Watson [19].

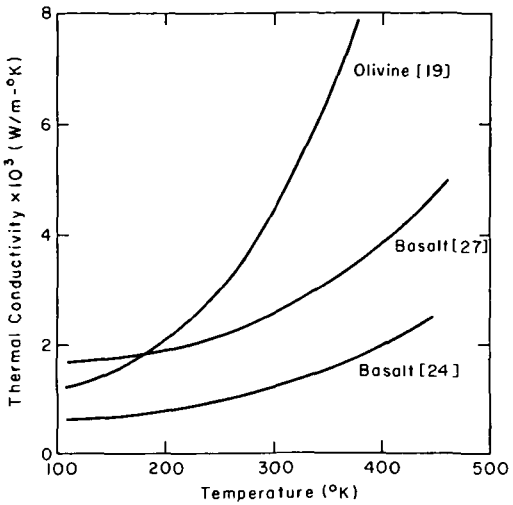

FIG. 3. Thermal conductivity of some evacuated terrestrial rock powders.

TABLE IV

THERMAL CONDUCTIVITY COEFFICIENTS A AND B FOR EQ. (10)

Material	Density (kg/m³)	A (W/m-°K)	B (W/m-°K⁴)	Ref.
Glass beads	1420	4.66×10^{-4}	2.99×10^{-11}	Wechsler and Simon [24]
	1380–1680	7.0	3.4	Watson [19]
Crushed quartz	1000	25.2	3.03	Wechsler and Simon [24]
	1220–1460	33.5	4.2	Watson [19]
Olivine	1370	10.9	12.6	Watson [19]
Basalt	1430	6.14	2.14	Wechsler and Simon [24]
	790	5.09	1.64	Fountain and West [27]
	1130	8.87	1.90	Fountain and West [27]
	1300	12.37	2.43	Fountain and West [27]
	1500	16.42	3.43	Fountain and West [27]
Apollo 11	1300	14.25	1.72	Cremers [38]
10084,68	1640	18.68	2.29	Cremers [38]
	1950	17.93	1.47	Cremers [38]
Apollo 12, 12001,19	1300	9.22	3.19	Cremers and Birkebak [37]
	1640	9.85	2.06	Cremers [40]
	1970	11.5	1.59	Cremers [41]
Apollo 14,	1100	8.36	2.09	Cremers [42]
14163,133	1300	6.19	2.49	Cremers [42]

TABLE V

THERMAL CONDUCTIVITY OF LUNAR FINES

Sample	Density (kg/m)	Temp. (°K)	Thermal conductivity (W/m-°K)	Ref.
Apollo 11, 10084,111	n.a.[b]	n.a.	1.05×10^{-3}	Bastin *et al.* [18]
	1300	n.a.	0.08	Ade *et al.* [31]
Luna 16	2300	n.a.	0.63	Vinogradov [33]
	2250	293–313	2.01	Avduevskii *et al.* [34]
Apollo 15, on site[a]	Variable	250	14–25	Langseth *et al.* [35]
Apollo 11, 10084,68	1300	298	1.88	Cremers *et al.* [32]
Apollo 12, 12001,19	1300	298	1.77	Cremers and Birkebak [37]
Apollo 14, 14163,133	1300	298	1.28	Cremers [42]

[a] Three determinations made, each at a different depth from the surface.
[b] Data not available.

However, the data given are too few and the scatter is too great to permit seeking a model such as Eq. (10) which will approximate the data.

The thermal conductivity of the lunar fines themselves have recently been determined by several investigators. The results are summarized in Table V. Bastin *et al.* [18] deduced the thermal conductivity of an "average" sample of Apollo 11 fines from the measured specific heat and previous remote measurements of microwave radiation absorption. Later, Ade *et al.* [31] from the same laboratory measured a much lower conductivity, perhaps using the same sample. They did not compare their second result with the first; however, they noted that their value was considerably less than that published by Cremers *et al.* [32]. They explain this by saying that the two determinations refer essentially to different situations. In one case the fines are put in a container, while in the other the mean conductivity of the top few centimeters of the surface of the moon is, in effect, determined in situ. A lower degree of compaction of the fines on the lunar surface and also the possibility of adsorbed gases at interparticle contacts in the laboratory determinations are both factors which could account for a discrepancy in the observed direction.

Vinogradov [33] and Avduevskii *et al.* [34] report thermal conductivity measurements on the same sample of material from the Luna 16 mission Their results differ by about a factor of three. No information is given as to methods of measurement.

Langseth *et al.* [35] made in situ measurements with the implanted heat

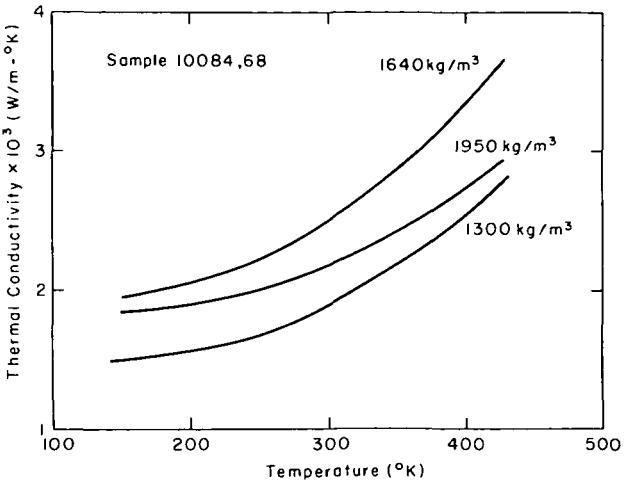

FIG. 4. Thermal conductivity of Apollo 11 fines.

flow probes at the Apollo 15 site. They report conductivities which are about a factor of ten greater than any others previously reported. The probe is described by Langseth *et al.* [36] and is essentially a ring heat source which is implanted in the surface layer by a driving mechanism. The time–temperature response of a sensitive resistance thermometer network in the probe is used to deduce the conductivity through solution of the governing temperature equation for the ring source.

Several individual points for the returned Apollo 11, 12, and 14 samples are given in Table V for purposes of comparison with the above data. These are part of a larger collection of data reported by Cremers and co-workers [32, 37–42]. The measurements reported in these papers were all made using the line heat-source technique described previously. In all cases Eq. (10) was found to represent the data adequately and the coefficients A and B are given in Table IV. The data as correlated by this expression are plotted in Figs. 4–6.

Curves for several densities are presented for each sample because, as explained previously, the effective thermal conductivity of a particulate medium is expected to be a function of density as well as temperature. The lowest density given in each case is that obtained with the lightest packing of the conductivity cell. This should represent the density of the upper centimeter or so of the lunar surface layer or in general the surface layer as ejected or moved and resettled without packing. Note that this density is 1300 kg/m³ for the Apollo 11 and 12 samples, but only 1100

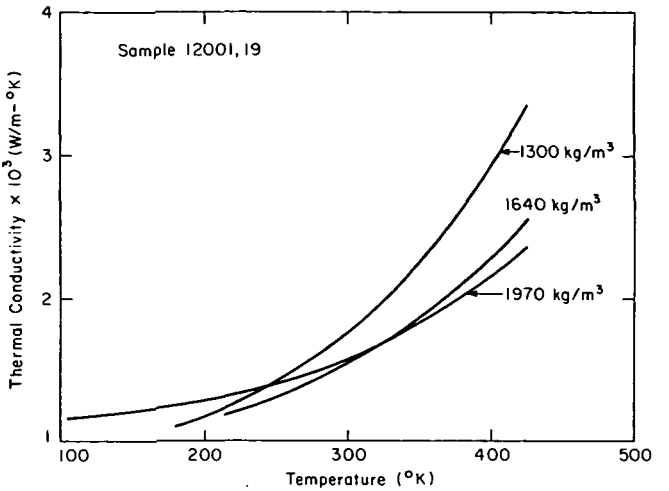

FIG. 5. Thermal conductivity of Apollo 12 fines.

kg/m³ for the Apollo 14 samples. Measurements on the Apollo 14 sample at densities greater than 1300 kg/m³ are in progress at present.

The intermediate density shown for the Apollo 11 and 12 samples, 1640 kg/m³, is the same as the average core-tube density for the Apollo 11 site as reported by Fryxell *et al.* [43], and so it should be close to the true surface

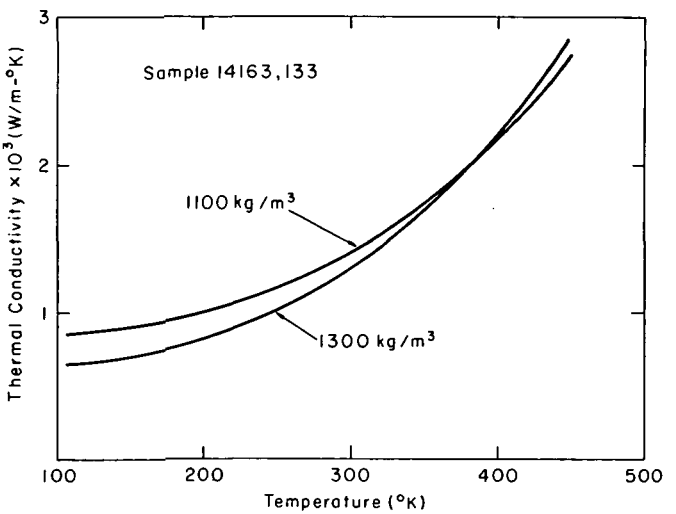

FIG. 6. Thermal conductivity of Apollo 14 fines.

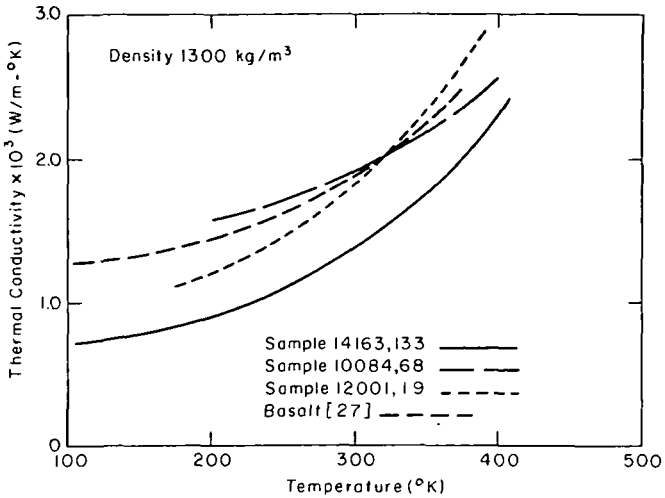

FIG. 7. Thermal conductivities of several lunar samples and terrestrial basalt at a density of 1300 kg/m³.

layer density at that location. The densities of 1950 and 1970 kg/m³ which are reported for the Apollo 11 and 12 samples respectively were the highest that could be obtained in the laboratory with these samples without resorting to extreme measures for packing. In the case of the latter sample, this was also approximately the average density of the core-tube sample as reported by Carrier *et al.* [44], and so it should be close to the true surface layer density at that location. The densities higher than the minimum in each case were arrived at by vibrating the test cell with a Vibrotool etching tool.

The lunar conductivity data are compared with one another and with the terrestrial basalt data of Fountain and West [27] in Fig. 7. The highest density given for the basalt was 1500 kg/m³ and so comparisons with this material at the higher densities used for the fines are precluded.

The differences from one curve to another are not too great when the data scatter is taken into account. As a measure of the scatter, an estimate of the error incurred in using Eq. (10) is given by the standard error of the estimate which is defined as

$$S = \left(\sum_{n=1}^{N} (k - k')^2 / N \right)^{1/2} \tag{12}$$

In Eq. (12), k represents the measured value at a given temperature and k' represents the value calculated at that temperature using Eq. (10). N is

the number of data points. In all cases reported by the author, S has been below 2×10^{-4} W/m-°K.

Differences in slope between the basalt data and those of the lunar fines probably represent the effects of different particle sizes and shapes rather than compositional differences. The basalt was sieved to a rather narrow size range of 37–62 μm, while the Apollo lunar fines varied in size from about 500 μm down to less than 1 μm with most of the particles at the low end of the range as reported by Gold *et al.* [45], King *et al.* [46], and Gold *et al.* [47]. The Apollo 12 fines appeared to be somewhat coarser and this observation was borne out in the size distribution measurements. This would tend to reduce the solid conduction component. A number of previous studies, including those mentioned above, have also shown that the fraction of glassy particles varies significantly from one site to another. The different internal structure and surface character of the glassy particles would affect both the conductive and radiative components of the effective conductivity.

Assessments of the thermal character of the lunar regolith frequently mention the ratio of radiative to conductive components of the effective thermal conductivity [e.g., 7, 20, 48]. This ratio has been predicted by a number of previous investigators for simulated lunar soil, and it is easily

TABLE VI

RATIO OF RADIATIVE TO CONDUCTIVE COMPONENTS OF EFFECTIVE THERMAL CONDUCTIVITY

Medium	Density (kg/m³)	Temp. (°K)	k_r/k_c	Ref.
Simulated lunar	—	350	1, 0.5[a]	Linsky [7]
Simulated lunar	—	300	1.08	Clegg *et al.* [20]
Simulated lunar	—	300	0.734	Winter and Saari [48]
Simulated lunar	—	350	1.17	Winter and Saari [48]
Basalt	1500	-350	0.895	Fountain and West [27]
Basalt	1500	100	0.021	Fountain and West [27]
Basalt	1130	350	0.918	Fountain and West [27]
Basalt	1130	100	0.021	Fountain and West [27]
Apollo 10084,68	1950	350	0.352	Cremers [38]
Apollo 10084,68	1950	100	0.008	Cremers [38]
Apollo 12001,19	1970	350	0.593	Cremers [41]
Apollo 12001,19	1970	100	0.014	Cremers [41]
Apollo 14163,133	1100	350	1.072	Cremers [42]
Apollo 14163,133	1100	100	0.025	Cremers [42]

[a] Values for dielectric constants of 2.5 and 1.5, respectively.

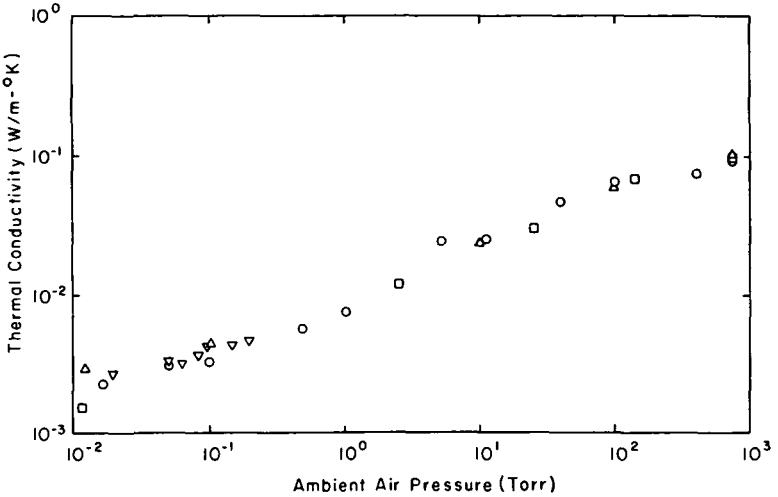

FIG. 8. Pressure effects on thermal conductivity. □ Sample 12001,19 [41], ○ sample 10084,68 [38], ▽ Luna-16 fines [34], △ terrestrial basalt [22].

calculated for actual samples once the coefficients of Eq. (10) are known. Some results for this ratio are given in Table VI. It is apparent that there is somewhat lower fraction of energy transmitted by radiation than by phonon conduction in the Apollo fines as compared with the basalt or soil models. As mentioned in the last paragraph, these differences are connected with variations in particle structure, size, and shape between the various samples or models.

The thermal conductivity of the lunar fines as a function of ambient pressure is shown in Fig. 8. The Apollo 11 data are for a density of 1640 kg/m^3, the Apollo 12 data are for a density of 1970 kg/m^3, the basalt data of Wechsler and Glaser [22] are for a density of 1270 kg/m^3, and the Luna-16 data of Avduevskii *et al.* [34] are for a density of 2250 kg/m^3. The agreement here is good. However, this is somewhat deceptive after considering the previous figures because this is a log–log plot. The increase in conductivity is almost a factor of 100 over the range of pressures given. It appears from this data and the data for other simulated lunar soils presented by Wechsler and Glaser [22] that the pressure effect is concentrated in the range above 10^{-2} Torr The conductivity has a constant value with respect to pressure below this level. This is evidenced by comparing the results at 10^{-2} Torr in Fig. 8 with those of Figs. 4–6 The latter data were obtained at pressures on the order of 10^{-5} Torr, and they are not substantially different from the 10^{-2} Torr data. The radiative transfer and

solid conduction apparently dominate the energy transfer at these low energy levels.

III. Specific Heat

A. LUNAR ROCKS

The specific heat of dielectric materials is primarily a function of molecular structure. It is a mass-specific property and so does not depend on density per se. However, because its magnitude depends on the available atomic and molecular energy storage mechanisms, it is a strong function of temperature. The measured values of this property for rocks do not vary greatly from one specimen to another for two reasons: (a) the major chemical constituencies of most representative rock materials are essentially the same, and (b) the calorimetric measurement of specific heat is quite refined.

Winter and Saari [48] plotted data for magnesium silicate, calcium feldspar, diabase, diorite, granite, basalt, silica glass, and quartz, and found that the data were adequately represented by the empirical equation

$$c = -34\,T^{1/2} + 8\,T - 0.2\,T^{3/2} \tag{13}$$

over the range of temperatures from a few degrees Kelvin to 400°K. The units of c in Eq. (13) are Joules per kilogram per degree Kelvin. Data presented by Bernett *et al.* [30] for silica sand and olivine are substantially in agreement with the representation given by Eq. (13). Robie *et al.* [17] suggest that this equation is useful ($\pm 10\%$) for substances having a mean atomic weight on the order of 20–21, but is not generally applicable for materials of different mean atomic weight.

Wechsler and Glaser [11, 22] present specific heats of basalt, pumice, and a number of other candidate materials for lunar surface layer simulation. Their results are average values over temperature ranges of several hundred degrees above room temperature. Data from Wechsler and Glaser [11] are included in Table I. All their data are in substantial agreement with that represented by Eq. (13).

The specific heats of a number of lunar rocks were measured by Robie and Hemingway [16] and Robie *et al.* [17] using a low temperature adiabatic calorimeter. They made their measurements over the approximate range of lunar diurnal temperatures and so the data are particularly valuable. The technique and apparatus are described in Robie *et al.* [17]. Measurements are presented for two Apollo 11 samples (vesicular basalt-10057 and breccia-10021) and one Apollo 12 sample (olivine dolerite-12018, 84). Their results are presented in Tables VII–IX and the envelope of the data is shown in Fig. 9. The correlation arrived at by Winter and

TABLE VII

EXPERIMENTAL SPECIFIC HEAT MEASUREMENTS FOR LUNAR SAMPLE 10057 (VESICULAR BASALT)[a]

Temp. (°K)	Specific heat (J/kg-°K)	Temp. (°K)	Specific heat (J/kg-°K)
96.43	258.7	231.55	632.9
103.54	274.6	239.78	645.5
111.50	296.0	247.68	660.1
120.38	324.8	255.59	676.0
129.30	352.5	263.63	689.0
137.57	379.7	271.93	703.7
145.76	405.6	280.23	717.9
154.71	432.4	288.28	730.5
163.10	457.9	293.21	738.4
171.35	483.9	301.01	748.5
179.25	506.5	309.16	762.7
186.82	530.4	316.53	771.1
199.29	549.2	325.72	782.8
201.87	568.5	333.76	792.0
209.68	583.9	341.59	805.0
217.74	601.5	348.44	814.2
255.75	617.0		

[a] From Robie *et al.* [17].

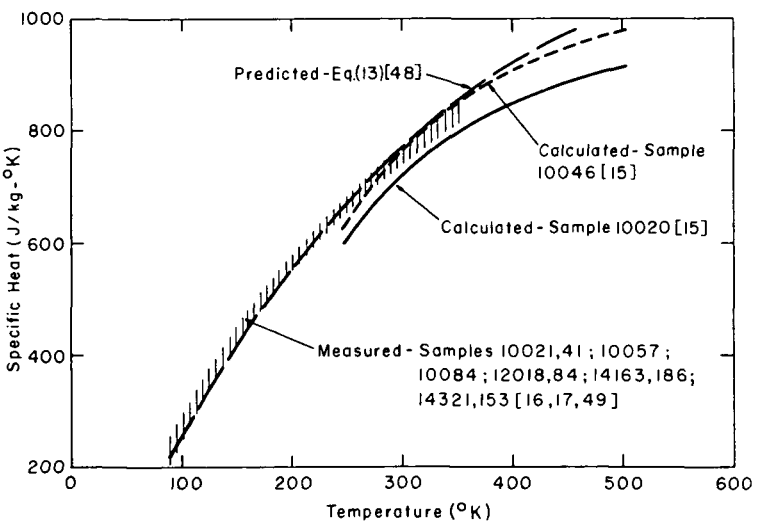

FIG. 9. Specific heats of lunar rocks and fines.

TABLE VIII

EXPERIMENTAL SPECIFIC HEAT MEASUREMENTS FOR LUNAR SAMPLE 10021,41 (BRECCIA)[a]

Temp. (°K)	Specific heat (J/kg-°K)	Temp. (°K)	Specific heat (J/kg-°K)
98.52	258.7	215.92	600.7
106.64	287.2	224.86	616.6
115.66	318.6	233.44	631.7
124.71	349.1	242.6	650.9
134.06	378.4	253.1	669.8
144.6	411.5	264.05	691.5
149.77	423.6	274.64	708.3
155.34	439.9	284.9	725.9
161.04	462.6	294.84	743.9
166.52	473.0	302.83	753.9
170.23	496.9	311.81	766.5
180.38	518.2	320.58	779.4
190.50	540.8	329.14	792.8
200.17	565.5	337.33	806.2

[a] From Robie and Hemingway [16].

TABLE IX

EXPERIMENTAL SPECIFIC HEAT MEASUREMENTS FOR LUNAR SAMPLE 12018,84 (OLIVINE DOLERITE)[a]

Temp. (°K)	Specific heat (J/kg-°K)	Temp. (°K)	Specific heat (J/kg-°K)
96.05	233.2	210.5	578.1
104.40	252.9	218.75	598.2
112.88	293.4	222.65	608.2
121.69	323.6	231.20	627.5
127.19	345.8	240.23	648.8
134.76	369.2	249.38	666.8
141.92	392.2	258.64	686.5
148.73	413.2	267.60	704.5
149.06	419.0	276.6	720.4
158.61	442.0	285.6	739.7
167.66	467.2	293.03	746.8
176.3	490.6	301.98	766.0
184.58	512.4	310.7	782.4
193.14	535.0	319.59	797.0
201.98	556.3	328.64	809.2

[a] From Robie and Hemingway [16].

TABLE X

EXPERIMENTAL SPECIFIC HEAT MEASUREMENTS FOR LUNAR SAMPLES 10017 (VESICULAR BASALT) AND 10046 (MICROBRECCIA)[a]

Rock 10017		Rock 10046	
Temp. (°K)	Specific heat (J/kg-°K)	Temp. (°K)	Specific heat (J/kg-°K)
2.344	1.934	3.08	1.172
2.393	1.950	3.26	1.758
2.472	1.921	3.32	1.465
2.713	2.022	3.54	1.884
2.876	2.034	3.71	1.59
3.028	2.085	4.05	1.005
3.399	2.214		
3.483	2.223		
3.819	2.340		
4.036	2.394		
4.27	2.545		
4.43	2.553		
4.52	2.679		
4.53	2.721		
4.54	2.637		
4.70	2.470		
4.97	2.805		

[a] From Warren *et al.* [14].

Saari [48], Eq. (13), is also shown for comparison. Note that the agreement is extremely good. As was noted before, this is to be expected.

Also shown on Fig. 9 are theoretical curves for the specific heats of a vesicular crystalline igneous rock (10020) and another breccia sample (10046). These curves are calculated from an expression derived by Horai *et al.* [15] using the known mineral composition of the samples and the thermodynamic data for these minerals. Again the agreement is quite good.

A single measurement on a third breccia sample (10065) by Bastin *et al.* [18] indicates a specific heat of 837 J/kg-°K. No information is given as to measurement method or sample temperature, and so presumably it is a room-temperature value.

The specific heat of lunar rock at extremely low temperatures was measured by Warren *et al.* [14] in their broader study of elastic and thermal properties. The results for two rocks (10017 and 10046) are given in Table X. The authors found that the measured specific heats did not agree with simple Debye theory which is valid for low temperatures. Using

this approach, the specific heat was calculated directly from the low temperature acoustic velocity, which was measured separately. However, the measured values were over 100 times larger than the predicted values.

Hemingway and Robie [49] recently published some smoothed values of the specific heat of an Apollo 14 breccia (14163, 186). These are also included in the data envelope in Fig. 9. It should be noted that the specific heats of samples from the Sea of Tranquility, the Ocean of Storms, and Fra Mauro are quite similar, being within 10% of one another at all temperatures between 100° and 400°K.

B. LUNAR FINES

The available specific heat measurements on lunar fines are considerably fewer than are those for the rocks. This is particularly true of simulated lunar fines. The reason for this being, of course, that there is substantially no difference between the specific heat of a rock and its powder. As all reasonable simulations involved powdered rock of one sort or another, the specific heat measurements were simply made on the parent rock.

TABLE XI

EXPERIMENTAL SPECIFIC HEAT MEASUREMENTS FOR LUNAR SAMPLE 10084 (FINES)[a]

Temp. (°K)	Specific heat (J/kg-°K)	Temp. (°K)	Specific heat (J/kg-°K)
95.17	268.7	299.00	619.5
99.56	278.0	231.49	627.5
105.16	291.8	233.93	627.9
112.25	313.1	239.78	642.1
119.98	336.1	246.27	651.3
127.19	358.3	253.83	664.7
134.50	382.2	262.18	681.1
142.83	401.9	270.31	695.7
152.61	445.4	278.22	710.8
162.69	473.4	285.93	721.7
167.02	478.9	293.46	727.1
176.27	507.3	300.84	740.1
185.10	528.3	308.07	750.1
193.60	548.8	327.71	784.0
202.94	574.7	332.70	794.9
213.07	594.4	337.93	798.3
222.84	615.3	343.43	802.9
224.85	614.9		

[a] From Robie *et al.* [17].

There are two sets of specific heat measurements available on the Apollo lunar fines. Robie *et al.* [17] measured the specific heat of Apollo 11 fines sample 10084. Their results are tabulated in Table XI. The data also fall into the envelope shown on Fig. 9. Hemingway and Robie [49] also presented some preliminary results on the Apollo 14 fines (14321, 153). These data also fall into the envelope. Note that there is very little difference between the specific heats of the fines and rocks.

Measurements on the Soviet Luna-16 fines reported by Vinogradov [33] show a specific heat of 712 J/kg-°K. No mention is made of the temperature for which this number is valid. Other measurements on the Luna-16 sample by Avduevskii *et al.* [34] show a specific heat of 741 J/kg-°K. The latter value is reported for the temperature range 273°–373°K. Both the Luna-16 values are in close agreement with the data of Robie *et al.* [17] and Hemingway and Robie [49].

IV. Thermal Diffusivity

A. Lunar Rocks

The thermal diffusivity is a transport property usually associated with transient heat transfer by conduction. It is defined as the thermal conductivity divided by the product of density times specific heat, or $\alpha = k/\rho c$. It usually appears explicitly in constant property analyses of transient heat conduction problems when the thermal conductivity can be factored from the heat conduction derivatives and is then divided by the ρc product from the energy storage term. As the thermal conductivity and specific heat of lunar media are both highly temperature dependent, the thermal diffusivity is of limited usefulness in analyses of lunar heat transfer.

Direct measurements of the thermal diffusivity of terrestrial geological materials abound in the literature. However, efforts to determine this property for candidate rocks for lunar simulation have been few. Usually the specific heat and thermal conductivity are measured along with the density of the material. Then the diffusivity is calculated from data such as those presented by Wechsler and Glaser [22].

The most extensive data available on the measured diffusivity of lunar rocks are presented by Horai *et al.* [15]. One set of these has already been presented in Table II; that for Apollo 11 rock 10057, a basalt. The other samples on which measurements are reported are 10020, a fine-grained vesicular crystalline igneous basalt like 10057, as well as 10046 and 10065, which are breccias.

The Angstrom method described by Kanamori *et al.* [50, 51] was used in the above measurements which covered a temperature range of 143°–

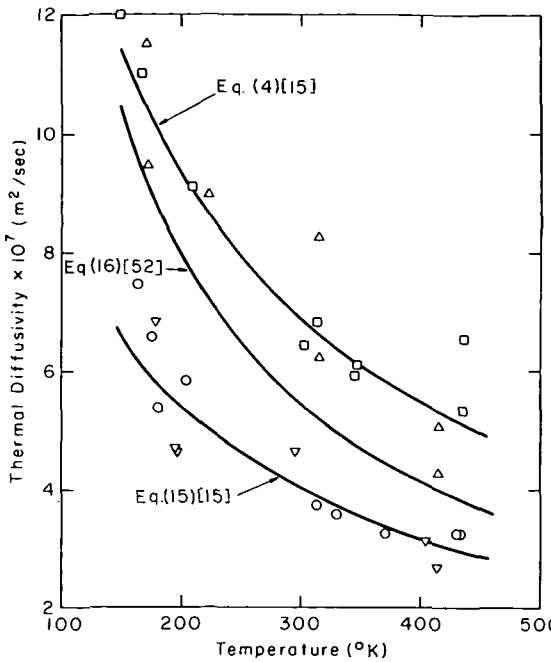

FIG. 10. Thermal diffusivity of lunar rocks from Apollo 11. Samples: △ 10020, □ 10057, ○ 10046, ▽ 10065.

423°K, approximately the range of lunar diurnal temperatures. All samples were rectangular prisms 1 × 1 × 2 cm in size. The thermal diffusivity was determined from the phase lag and the amplitude decay with distance of a periodic temperature wave. The geometry used was one in which the temperature wave propagates through the specimen in the direction perpendicular to the long axis of the prism. Dow Corning-4 heat sink compound was used to obtain good thermal contact between the sample and heater and between the sample and the thermocouple.

A temperature wave of 5°–15°K in amplitude and 0.008–0.02 Hz in frequency was found to be adequate for the above measurements. A dc component of the temperature wave heated the samples about 100°K above the ambient temperature which was controlled by either liquid nitrogen or solid carbon dioxide in order to obtain the desired sample temperature. The results of the measurements are given in Table XII in addition to those already given in Table II. The data are plotted against temperature in Fig. 10. Also shown are least-squares curves giving the diffusivity as an inverse function of temperature, a relationship which is

TABLE XII

THERMAL DIFFUSIVITY OF APOLLO 11 LUNAR MATERIAL

Sample	Temp. (°K)	Frequency of temp. wave (Hz)	Thermal diffusivity (m^2/sec)
10020	171	2.0×10^{-2}	9.48×10^{-7}
	173	1.5	10.75
	222	1.2	8.99
	315	1.0	8.29
	315	1.5	6.21
	414	2.0	4.26
	415	1.0	4.91
10057	149	2.0×10^{-2}	11.94×10^{-7}
	166	1.5	11.03
	208	1.5	9.06
	304	1.5	6.44
	313	1.0	6.86
	344	1.5	6.06
	345	2.0	5.91
	435	1.2	5.37
	436	0.8	6.55
10046	162	0.8×10^{-2}	7.47×10^{-7}
	176	0.8	6.59
	181	1.0	5.37
	205	0.8	5.85
	313	0.9	3.75
	330	0.7	3.60
	371	0.8	3.28
	430	0.9	3.26
	433	0.8	3.25
10065	178	0.8×10^{-2}	6.83×10^{-7}
	190	1.0	4.72
	191	1.2	4.65
	295	0.8	4.63
	404	0.8	3.15
	414	0.9	2.69

appropriate for many solids. These are

$$\alpha^{-1} = 0.378 \times 10^4 T + 0.314 \times 10^6 \tag{14}$$

for the fine-grained vesicular crystalline igneous rocks, 10020 and 10057, and

$$\alpha^{-1} = 0.648 \times 10^4 T + 0.595 \times 10^6 \tag{15}$$

for the breccias, 10046 and 10065.

Horai *et al.* [52] measured the thermal diffusivity of two Apollo 12 rocks, samples 12002 and 12022, both of which are crystalline igneous rocks (olivine dolerite). They found an almost identical variation of thermal diffusivity with temperature for the two rocks which is given by the empirical relation

$$\alpha^{-1} = 0.58 \times 10^4 T - 9.0 \times 10^4 \quad (16)$$

The data show that the diffusivity of the Apollo 12 rocks is more temperature dependent than that of the Apollo 11 crystalline rocks. The authors relate this to the higher olivine and pyroxene contents of the former. Equation (16) is also shown on Fig. 10 for comparison.

Mizutani *et al* [53] measured the thermal diffusivity of Apollo 14 sample 14311,50 which is identified as a polymict fragmental rock. The measurements were made in air at atmospheric pressure and at 10^{-3}–10^{-5} Torr using the modified Angstrom method of Kanamori *et al.* [51] again. The results and best-fit curves are shown in Fig. 11. The thermal diffusivity was found to be substantially lower under vacuum than in atmospheric air. The possible reason is suggested wherein gas in microcracks and pores contributes significantly to the heat transfer at higher pressures. The authors suggest that the low values of vacuum thermal conductivity due to microcracks and pores may be significant in the

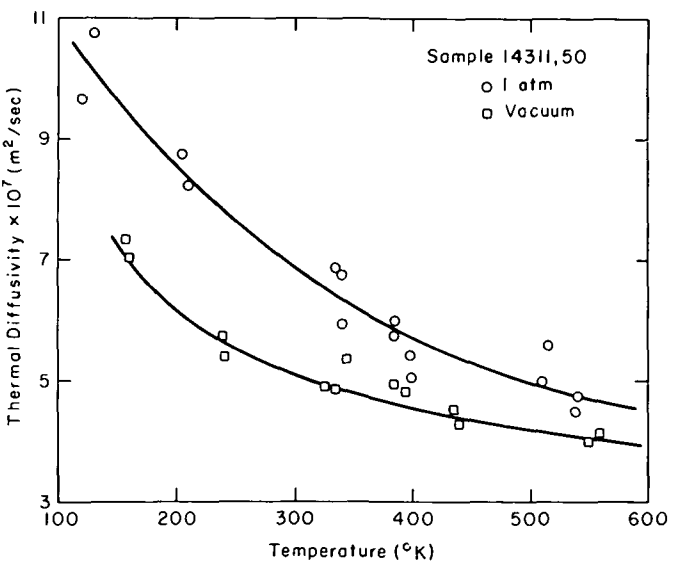

FIG. 11. Thermal diffusivity of lunar rock from Apollo 14.

thermal evolution of the moon because these discontinuities may persist to a fairly deep level owing to the low pressure in the moon.

B. LUNAR FINES

There are, to the author's knowledge, no direct measurements of the thermal diffusivity of either simulated or actual lunar fines. However, there have been several calculated values for both classes of sample.

Wechsler and Glaser [22] calculated the thermal diffusivity of glass microbeads, expanded perlite, pumice powder, basalt powder, and granite powder from separate measurements of thermal conductivity and specific heat. Their results for vacuum conditions on the order of 10^{-1} Torr and below are summarized in Table XIII. Here, in many cases, average values for several runs are recorded. Also shown are some data presented by Bernett *et al.* [30] for powdered basalt.

It is not possible to calculate the thermal diffusivity for the Apollo 11 conductivity data of Bastin *et al.* [18] and Ade *et al.* [31] as these are not accompanied by corresponding density values that would permit such a

TABLE XIII

THERMAL DIFFUSIVITY AND THERMAL PARAMETER OF SIMULATED LUNAR FINE MATERIALS[a]

Material	Density (kg/m^3)	Temp. (°K)	Thermal diffusivity (m^2/sec)	Thermal parameter (m^2-°K-$sec^{1/2}/J$)
Glass beads [150 μ]	1460	298	3.9×10^{-9}	1.25×10^{-2}
Glass beads [50 μ]	1460	298	2.3	1.63
Glass beads [29 μ]	1460	298	2.0	1.76
Expanded perlite	137	298	12.7	8.18
Pumice	877	277	2.80	2.73
Pumice	877	328	3.22	2.21
Pumice	877	296	2.05	3.27
Granite	1130	297	2.22	2.24
Granite	1130	353	2.65	2.08
Basalt	1270	283	1.9	2.16
Basalt	1270	331	2.34	1.83
Basalt	1270	221	2.04	2.32
Basalt	1570	213	1.1	1.28
Basalt	1570	273	1.0	1.63
Basalt	1570	363	1.05	1.43

[a] First twelve entries in table are from Wechsler and Glaser [22]; last three entries are from Bernett *et al.* [30].

TABLE XIV

COEFFICIENTS FOR CALCULATING SMOOTHED VALUES OF THERMAL DIFFUSIVITY OF LUNAR FINES FROM:
$\alpha = b_0 + b_1T + b_2T^2 + b_3T^3 + b_4T^4$ (m^2/sec)

Sample	Density (kg/m^3)	$b_0 \times 10^9$	$b_1 \times 10^{11}$	$b_2 \times 10^{13}$	$b_3 \times 10^{16}$	$b_4 \times 10^{19}$
Apollo 11[a]	1300	1.099	−1.145	5.501	−1.195	0.999
Apollo 11[a]	1640	1.142	−1.190	5.714	−1.241	1.037
Apollo 11[a]	1950	0.915	−0.945	4.478	−0.960	0.783
Apollo 12[b]	1300	0.707	−0.731	3.52	−0.742	0.622
Apollo 12[b]	1640	0.601	−0.624	3.00	−0.645	0.540
Apollo 12[b]	1970	0.586	−0.610	2.93	−0.635	0.531

[a] Sample 10034,68 from Cremers [38]. [b] Sample 12001,19 from Cremers [41].

calculation. However, the specific heat data of Robie *et al.* [17] can be used with the conductivity data of Cremers *et al.* [32, 37–41] to calculate the thermal diffusivity over the approximate range of lunar temperatures. It should be noted that the specific heat data are valid only for the Apollo 11 fines. However, evidence previously cited indicates that all the lunar fines should have substantially the same specific heats. The thermal diffusivities for the Apollo 11 (10084, 68) and Apollo 12 (12001, 19) are plotted in Figs. 12 and 13, respectively.

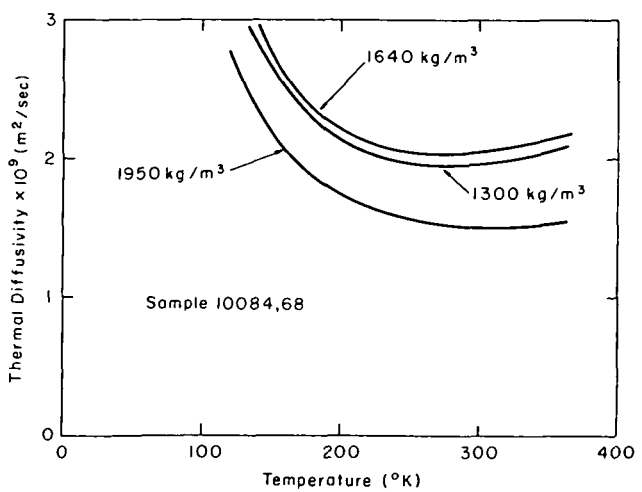

FIG. 12. Thermal diffusivity of fines from Apollo 11.

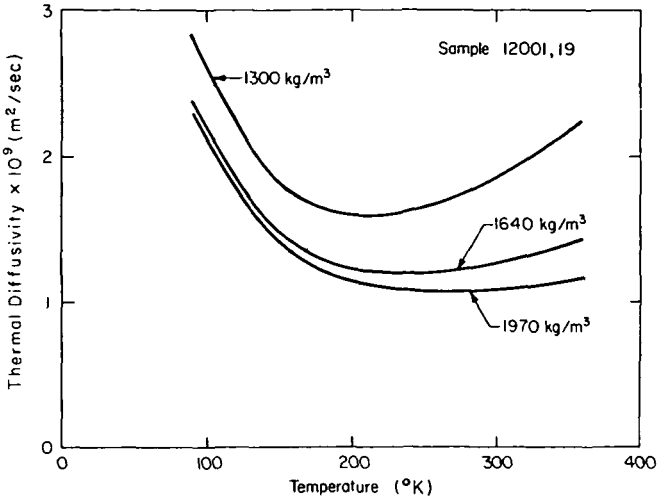

FIG. 13. Thermal diffusivity of fines from Apollo 12.

The curves shown in Figs. 12 and 13 are fourth-order polynomials fitted to the diffusivity data calculated from the smoothed thermal conductivity values of Cremers *et al.* [37–41] and the smoothed specific heat data of Robie *et al.* [17]. The resultant coefficients of curves which are displayed are given in Table XIV for the Apollo 11 and Apollo 12 samples.

The thermal diffusivity of the Luna-16 sample can be calculated from the two sets of specific heat and conductivity data previously mentioned. The data of Vinogradov [33] indicate a diffusivity of 1.34×10^{-9} m²/sec, which is presumably valid for room-temperature conditions (297°K), while the data of Avduevskii *et al.* [34] indicate a diffusivity of 1.2×10^{-9} m²/sec for the temperature range 293°–313°K. These values are close to those for the Apollo 12 fines presented in Fig. 13.

V. Thermal Parameter

Constant property analyses of heat conduction problems in which the boundary conditions are periodic with time are often cast in terms of the thermal parameter [54]. This property is defined as

$$\gamma = (k\rho c)^{-1/2} \tag{17}$$

It can be shown that for many problems the amplitude of the heat flux variation at any position is proportional to γ^{-1}. One such problem is that of a semiinfinite solid such as the lunar surface under periodic solar heating. Consequently, it can be expected that the amplitude of the temperature

TABLE XV

THERMAL PARAMETER OF LUNAR SURFACE LAYER

Reference	Thermal parameter $\times 10^2$ (m^2-°K-$sec^{1/2}$/J)	Source
Wesselink [4]	2.39	Compared with IR eclipse data of Pettit [3]
Jaeger [5]	1.20	Compared with IR eclipse data of Pettit and Nicholson [2]
Krotikov and Troitsky [6]	0.84	Compared with own radio measurements
Linsky [7][a]	1.60–2.12	Compared with radio measurements of Krotikov and Troitsky [6]. Variable property model with dielectric constant of 2.5
Linsky [7][a]	2.33–2.46	Compared with radio measurements of Krotikov and Troitsky [6]. Variable property model with dielectric constant of 1.5
Linsky [7][a]	0.60–2.57	Compared with radio measurements of Krotikov and Troitsky [6]. Two-layer model of constant properties
Linsky [7][a]	1.10–2.57	Compared with radio measurements of Krotikov and Troitsky [6]. Two-layer model of constant properties
Linsky [7][a]	1.60–2.12	Compared with IR eclipse data of Pettit [3]
Lucas *et al.* [63]	0.60–3.11	Compared with temperature data from Surveyor spacecraft
Muncey [56][b]	0.48–0.72	Compared with IR eclipse data of Pettit and Nicholson [2]. Variable property model
Murray and Wildey [61][c]	1.91, 0.72	Compared own IR data with prediction of Jaeger [5]
Low [62]	2.39	Compared own IR data with prediction of Wesselink [4]
Avdeuvskii *et al.* [34]	1.73	Calculated from properties of Luna-16 sample, $\rho = 2250$ kg/m^3
Cremers [41][d]	3.95, 1.84	Calculated from properties of Apollo 12 sample, $\rho = 1970$ kg/m^3

[a] Evaluated at 350°K. [b] Evaluated at 300°K. [c] Nighttime and sunset values, respectively. [d] Evaluated at 100° and 350°K, respectively.

variation on the moon will be a strong function of the thermal parameter.

Sufficient data have been presented in the preceding sections to permit the calculation of the thermal parameter for any temperature, and so the results of such calculations will not be repeated here. In Section VII, suggested reference values of this property will be presented for use in constant property analyses. There is reason, however, for discussing this property further from a historical viewpoint.

Until the moon landings, all thermal analyses of the lunar surface layer had to proceed with the use of physical properties of an assumed medium. The results of these analyses were then compared with remote infrared or microwave radiation measurements made from earth. The values of the thermal parameter which gave the best agreement between prediction and remote measurement were then used to infer the character of the lunar surface layer. It was known, for instance, as early as 1948 [4] that the lunar surface was covered with a layer of porous material. However, whether it was a solid matrix or powdery one was not known for certain until the Surveyor series of flights.

It has already been noted that the thermophysical properties of the moon are highly temperature dependent. Consequently, the thermal parameter will also be a function of temperature and a nonlinear one at that. This explains why it was difficult for past investigators to get complete agreement between the constant property predictions and the remote measurements. For instance, it is pointed out in the recent work by Winter and Saari [48] that for constant property models a thermal parameter of 0.0311 m^2-°K-$sec^{1/2}$/J is achieved by matching theory with experimental data during the umbral phase of an eclipse. However, this leads to unacceptably low calculated values of lunar nighttime temperatures. When γ is set equal to 0.0191 to reproduce measured nighttime temperatures, there is substantial disagreement with eclipse measurements.

Some estimated values of the thermal parameter from the literature are given in Table XV. These were obtained by comparing lunar temperatures deduced from radiation measurements with those predicted by constant property theory. Also included are values calculated from the measured properties of the Apollo 12 fines at a density of 1970 kg/m^3 for a typical daytime temperature of 350°K and also for a typical nighttime temperature of 100°K. The thermal conductivity and specific heat for these calculations are taken from Figs. 5 and 9 respectively.

VI. Heat Transfer in the Lunar Surface Layer

A number of investigators [4, 5, 54–56] have calculated surface temperatures at the lunar equator using constant thermophysical properties

obtained for an assumed medium. Others have suggested certain models for the temperature variation of the thermal conductivity and specific heat without making calculations of the actual temperature distribution. The most advanced work previous to the Apollo program has been done using measured values of the thermophysical properties of an assumed medium [7, 19, 48, 57–59]. The merit of this work lies more in what the investigators inferred about the moon than in the temperatures which were calculated. The temperature distributions were compared with those obtained from earth-based microwave and infrared measurements. Excellent working models for the lunar surface layer were constructed from which thermal and mechanical calculations could be carried out.

Many previous papers [2, 60–62] have reported direct, although remote, measurements from which the lunar surface temperature was calculated. Photometric scans of the lunar disk during eclipses or lunar nighttimes were made through several infrared and microwave windows in the atmospheric absorption spectrum. All lunar radiation in the absence of sunlight is emitted radiation, and so the temperature can be evaluated using the Planck distribution law. These measurements yield spatially integrated values of the lunar emission over areas on the order of 20–50 km in diameter. This can cause some difficulty in interpretation because of the known existence of thermal anomalies on the moon caused either by density variations in the surface layer or by significant local heat flow from the lunar interior.

The only localized experimental determinations of the temperature of the lunar surface before Apollo have been obtained through an ingenious application of the heat balance to spacecraft components. These experiments are summarized in Lucas *et al.* [63], Vitkus *et al.* [64–66], and Stimpson and Lucas [67]. The temperatures of two component-panels of the Surveyor I, III, V, VI, and VII landing vehicles were obtained by analyzing data telemetered from the vehicles. These temperatures were then used in a heat balance involving conduction through components and radiation exchange between the panels and the lunar surface as well as with other components of the spacecraft. An error analysis on the calculations showed that the nighttime temperatures were accurate to within 8°K, while the daytime temperatures were good to within 12°–40°K, depending on sun angle. The longest time period covered was about two-thirds of a lunar day. This was done on the Surveyor V mission.

The Apollo 13 flight was the first lunar mission which carried a probe for direct measurement of the temperature in the lunar surface layer. The flight was aborted on the way to the moon because of a system malfunction and consequent failure.

Two probes were later included on the Apollo 15 flight and were success-

fully implanted on the moon. The probe design is described by Langseth *et al.* [36], and the Apollo 15 results are described by Langseth *et al.* [35] The temperature measured 1 m below the surface was 250.7°K at one probe and 252.3°K at the other probe. Both values are at least 25°K higher than mean temperatures calculated for constant density models. The steady temperature gradient at depths where the temperature variations caused by lunation and damped out was measured to be 1.75°K/m. The average heat flow through the surface layer is estimated from these measurements to be 3.3×10^{-2} W/m^2. This is about half the value of the heat flow from the earth's interior.

The return and analysis of the Apollo 11 and 12 samples has permitted, for the first time, the calculation of the temperature distribution in the lunar surface layer retaining the full parametric dependencies of the properties of the regolith. These include the temperature and density dependence of the thermal conductivity, specific heat, and surface emittance, and the density and angular dependence of the surface reflectance.

Consideration of heat transfer in a porous evacuated medium makes it possible to establish a rather straightforward model for energy transfer in the lunar surface layer. Because of the excellent insulating qualities of evacuated rock powders, the depth to which there will be significant daily temperature variation is on the order of a meter, whereas the moon's diameter is on the order of 3×10^6 m. Therefore, the heat flow can be considered as one-dimensional in a Cartesian coordinate system. The energy equation is then expressed as

$$\rho c(T) \frac{\partial T}{\partial t} = \frac{\partial}{\partial x}\left(k(T) \frac{\partial T}{\partial x}\right) \tag{18}$$

In Eq. (18) it is assumed that the specific heat and thermal conductivity are explicit functions of temperature and that the density is constant with depth. The latter assumption is borne out by observations made by the Apollo 12 astronauts and reported in reference [8]. However, this is at variance with the arguments of Langseth *et al.* [35] which explain the anomalously high heat flux measured by probe at the Apollo 15 site.

It is convenient to express Eq. (18) in terms of dimensionless variables. Because the problem is periodic, it is convenient to make the time dimensionless with the period of lunation P which is 2.55143×10^6 sec so that $\tau = t/P$. The length variable x is made dimensionless with the wavelength of the first fundamental wave of the constant property solution of Eq. (18). That is, $\xi = x/(4\pi\alpha^* P)^{1/2}$. Here α^* is the thermal diffusivity evaluated at the average lunar temperature, that is, the temperature far below the moon's surface. The dimensionless equation can then be expanded and

written as

$$\frac{\partial T}{\partial \tau} = \frac{\alpha}{4\pi\alpha^*}\left[\frac{1}{k}\frac{dk}{dT}\left(\frac{\partial T}{\partial \xi}\right)^2 + \frac{\partial^2 T}{\partial \xi^2}\right] \tag{19}$$

where k and α are both functions of temperature. Consideration must now be given to the boundary conditions on Eq. (19).

The condition at large depth to be imposed on Eq. (19) is that the heat flux goes to zero. The Apollo 15 heat-flux probe has shown that the average lunar heat flux is much less than that caused by insolation and cooling near the surface. In addition it is required that the problem be periodic with a period already mentioned.

The condition at the surface is expressed by a heat balance between the incoming solar radiation and the energy which is emitted to space, plus that which is conducted into the surface layer. As the sun's angle with respect to the normal varies during the day, the fraction of incoming radiation which is absorbed also changes. These conditions are written as

$$\xi = 0, \qquad I(\tau) = \epsilon(T)\sigma T_0^4 - k(T)\left.\frac{\partial T}{\partial \xi}\right|_{\xi=0} \tag{20}$$

The insolation term is

$$I(\tau) = S[1 - r(\tau)]\cos\Lambda\cos[\beta + 2\pi\tau] \tag{21}$$

during the half-period of daytime, and $I(\tau) = 0$ during the half-period of nighttime. In Eq. (20), ϵ is the total hemispherical emittance which is a function of temperature, and in Eq. (21), $r(\tau)$ is the directional reflectance which will vary with the sun's angle of incidence, and so it can be expressed as a function of the time variable τ. Λ is the latitude and β is longitude of the lunar site in question. S is the solar constant which was taken as 1395 W/m^2 [68]. Recent measurements indicate that 1353 W/m^2 is perhaps a better value to use [69].

Equation (19) was solved on the IBM 360-65 digital computer using a modified Runge–Kutta scheme. Initially, the directional reflectance and temperature dependent emittance were not available for use in Eqs. (20) and (21). Results for the Apollo 11 and 12 sites for constant values of these properties are given by Cremers *et al.* [70] and Cremers *et al.* [71]. The noon, sunset, midnight, and sunrise temperatures are given in Table XVI.

Later, when the directional reflectance and temperature dependent emittance became available, Cremers *et al.* [39] recalculated the Apollo 12 temperatures. The effect of a directionally dependent reflectance should be significant because if a constant reflectance is assumed, the surface immediately begins absorbing a given fraction of radiation at sunrise and

TABLE XVI

COMPARISON OF MEASURED AND CALCULATED LUNAR SURFACE TEMPERATURES (°K)[a]

Source	Noon	Sunset	Midnight	Sunrise
Apollo 11 Cremers [38]	395	152	101	92.9
Apollo 11 Cremers [41]	389	134	95	86.1
Wesselink [4]	370	144	98	90
Jaeger [5]	368	178	97	89
Linsky [7]				89
Pettit and Nicholson [2]	374		120	
Sinton [55]	389	181	122	109
Saari [72]			104	
Low [62]				90
Ingrao *et al.* [73]	393			
Stimpson and Lucas [67]	386–390	140–200	100–112	

[a] From Cremers *et al.* [70].

continues absorbing this fraction until sunset. In the real case, however, at grazing angles the reflectance is near unity and so there is little absorption. Inclusion of the directional dependence of the reflectance has the important effect of moderating changes between night and day temperatures in periods near sunset and sunrise.

The results obtained for the complete variable property case for the Apollo 12 site are given in Fig. 14. A comparison between temperatures from the present study and the results of the above analysis in which the reflectance and emittance were held constant at mean values is given in Table XVII and by the dashed line in Fig. 14. Note that at noon there is practically no difference because the sun is directly overhead and the normal reflectance was that used in the constant surface property analysis. The only difference between the two calculations is in the emittance. The really significant differences in the two models are just before sunset and just after sunrise. The maximum differences occur at $\tau = 0.24$ where the temperature is lower by 43.7°K in the variable property case and at $\tau = 0.76$ when the temperature is lower by 64.1°K in the variable property case.

The temperatures at the Apollo 12 site were compared in Table XVI with those calculated for the Apollo 11 site. It should be reemphasized that there were no total directional reflectances or temperature dependent emittances available when the latter calculations were made, and so constant radiative properties were assumed. The generally lower temperatures in the Apollo 12 case are due primarily to the lesser amount of energy

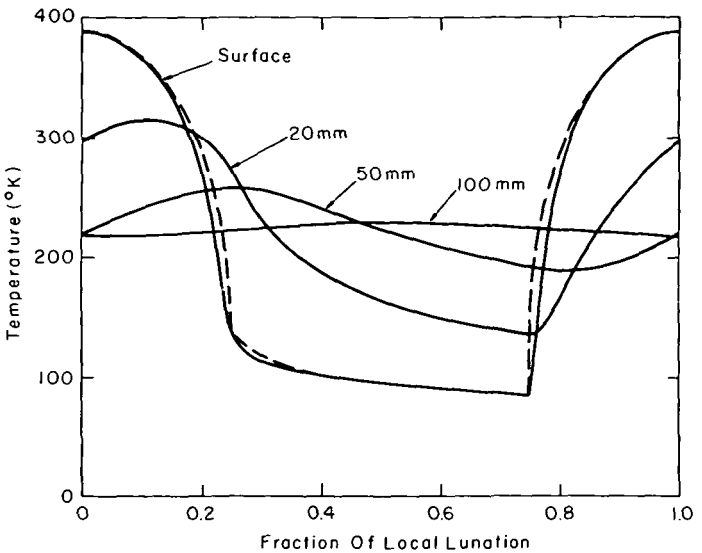

FIG. 14. Temperature variation on the moon during a lunation.

calculated to be absorbed during the day. This difference is caused by taking the directional dependence of reflectance into account. The most significant differences occur again just before sunset and just after sunrise when the constant surface property model deviates the most from the actual situation. The differences in conductivity and diffusivity become

TABLE XVII

COMPARISON OF TEMPERATURES FOR THE CASE OF VARIABLE SURFACE PROPERTIES WITH THAT OF CONSTANT SURFACE PROPERTIES[a]

Time	Temperature (°K)	
	Variable r, ϵ	Constant r, ϵ
0 (Noon)	389.3	389.4
0.24	161.2	204.9
0.25 (Sunset)	134.4	147.5
0.50 (Midnight)	94.7	96.8
0.75 (Sunrise)	86.1	87.8
0.76	125.4	189.5

[a] From Cremers *et al.* [39].

most apparent beneath the surface. The amplitude of the diurnal variation at depths of 20 and 50 mm is on the order of 20°K greater in the Apollo 11 case.

It is of historical interest to compare the present results with some prior calculations of lunar temperatures which were based on assumed properties. These calculations were usually made in terms of the thermal parameter. For the studies of Cremers *et al.* [39, 70, 71], the value of the thermal parameter based on reference properties (discussed in Sect. VII) is about 2.4×10^{-2} in SI units. For comparison, temperatures were calculated by Wesselink [4] ($\gamma = 0.28 \times 10^{-2}$), Jaeger [5] ($\gamma = 2.39 \times 10^{-2}$), and Linsky [7] ($\gamma = 2.39 \times 10^{-2}$), among others. Wesselink and Jaeger assumed constant properties throughout, and the numbers taken from Linsky were calculated for an assumed medium with temperature dependent specific heat and thermal conductivity. The results of these calculations are given in Table XVI along with those from calculations based on the Surveyor studies.

Also shown in Table XVI are the results of remote measurements of lunar surface temperatures. These include temperatures inferred from measurements of infrared or microwave radiation during lunar nighttimes or during eclipses by Pettit and Nicholson [2], Sinton [55], Saari [72], Low [62], Ingrao *et al.* [73], and Stimpson and Lucas [67]. In the latter paper several

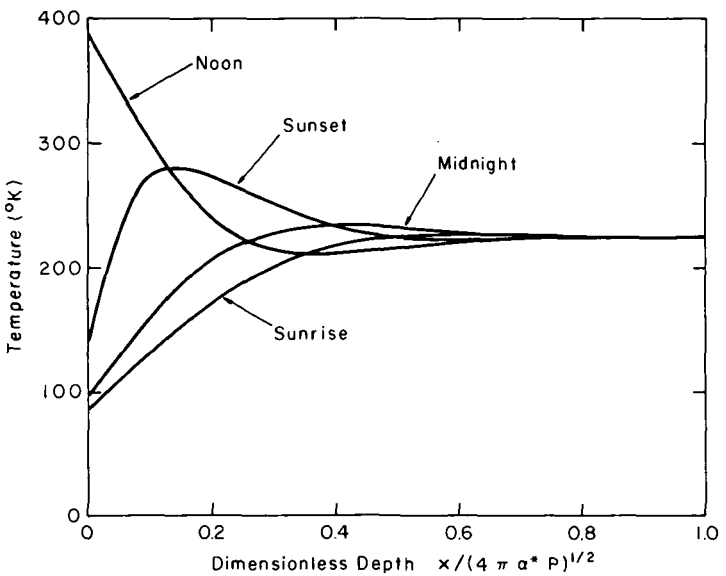

FIG. 15. Temperature variation on the moon as a function of depth.

separate determinations are made of each temperature and the results are presented here as a range. Considering the assumptions required to deduce temperatures from the data and the wide area from which the measured radiation originates, the agreement is quite good.

Figure 15 shows the variation of temperature with depth for several times during the lunar day as calculated from Eq. (19). It is seen that the temperature wave damps out rapidly with distance because of the excellent insulating characteristics of the lunar surface material. In both the Apollo 11 and 12 cases, the daily variation in temperature drops to about 1° at about $\xi = 0.85$ which corresponds to a depth of only 0.172 meters. The steady temperature on the moon below this depth is 225°K, considerably below that measured for the Apollo 15 site.

VII. Reference Values of Thermophysical Properties

It is frequently of interest to have relevant reference values of the thermophysical properties available for computational convenience because in many analyses the constant property assumption will suffice. There are two ways of calculating meaningful reference properties for the typical lunar problems. One way is to calculate the integrated average of the property in question over the temperature range of interest. That is, for a

TABLE XVIII

AVERAGE VALUES OF THERMAL CONDUCTIVITY, THERMAL DIFFUSIVITY, AND THERMAL PARAMETER FOR THE APOLLO FINES SAMPLES[a]

Density (kg/m³)	Thermal conductivity (W/meters-°K)		Thermal diffusivity (m²/sec)		Thermal parameter (m²-°K-sec$^{1/2}$/J)	
	$\bar{k} \times 10^3$	$k^* \times 10^3$	$\bar{\alpha} \times 10^9$	$\alpha^* \times 10^9$	$\bar{\gamma} \times 10^2$	$\gamma^* \times 10^2$
Apollo 11						
1300	1.77	1.61	2.34	2.04	2.73	2.81
1640	2.32	2.12	2.42	2.11	2.12	2.17
1950	2.09	1.95	1.85	1.64	2.06	2.08
Apollo 12						
1300	1.52	1.28	1.95	1.58	2.91	3.11
1640	1.37	1.21	1.44	1.21	2.77	2.87
1970	1.45	1.33	1.29	1.08	2.48	2.47

[a] From Cremers *et al.* [38, 41].

property $p(T)$ the integrated average $\bar{p}$ is given by

$$\bar{p} = (T_{\max} - T_{\min})^{-1} \int_{T_{\min}}^{T_{\max}} p(T)\, dT \tag{22}$$

In Eq. (22) $T_{\max}$ and $T_{\min}$ are the extreme temperatures of the problem. A second way is to simply evaluate the property at a mean value of temperature. That is, $p^* = p(\bar{T})$. The obvious temperature to use here is the average temperature of the lunar surface layer. As the properties k, α, and c of the lunar fines are nonlinearly dependent on temperature, there will be a difference in the two sets of calculations

Cremers [38, 41] carried out the reference property calculation for the Apollo 11 and 12 fines samples. The results are given in Table XVIII. The temperatures used are taken from Cremers *et al.* [39, 70], respectively.

ACKNOWLEDGMENTS

The author wishes to express his gratitude to the National Aeronautics and Space Administration for financial support for the investigations of lunar thermophysical properties. Many thanks are also due to Beverly Martin and Lynda Young who typed the manuscript and to Carla Cremers who helped organize much of the author's own data as well as those of others.

NOMENCLATURE

A	Coefficient of Eq. (10)
B	Planck blackbody function; coefficient of Eq. (10)
c	Specific heat
I	Insolation
J	Radiative intensity
k	Thermal conductivity
P	Period of cyclic heat flux
q	Heat flux per unit length
Q	Heat flux per unit area
r	Surface reflectance
s	General direction
S	Solar constant
t	Time
T	Temperature
x	Distance from surface

GREEK SYMBOLS

α	Thermal diffusivity
α^*	Thermal diffusivity at average lunar temperature
β	Longitude
γ	Thermal parameter $(k\rho c)^{-1/2}$
ϵ	Surface emittance
θ	Angle from surface normal
κ	Absorption coefficient
Λ	Latitude
ξ	Dimensionless distance $x/(4\pi\alpha^* P)^{1/2}$
ρ	Density
τ	Dimensionless time t/P

SUBSCRIPTS

c	Conduction
r	Radiation
ν	Frequency
0	Surface

REFERENCES

1. P. Epstein, *Phys. Rev.* **33**, 269 (1929).
2. E. Petitt and S. B. Nicholson, *Astrophys. J.* **71**, 102 (1930).
3. E. Pettit, *Astrophys. J.* **91**, 408 (1940).

4. A. J. Wesselink, *Bull. Astron. Inst. Neth.* **10**, 351 (1948).
5. J. C. Jaeger, *Aust. J. Phys.* **6**, 10 (1953).
6. V. D. Krotikov and V. S. Troitsky, *Sov. Astron.—AJ.* **6**, 841 (1963).
7. J. L. Linsky, *Icarus* **5**, 606 (1966).
8. "Apollo 11 Preliminary Science Report" *NASA Spec. Publ.* **NASA SP-214** (1969).
9. "Apollo 12 Preliminary Science Report"*NASA Spec. Publ.* **NASASP-235** (1970).
10. "Apollo 14 Preliminary Science Report" *NASA Spec. Publ.* **NASA SP-272** (1971).
11. A. E. Wechsler and P. E. Glaser, *Icarus* **4**, 335 (1965).
12. D. R. Stephens, High Temperature Thermal Conductivity of Six Rocks. Univ. of California, Lawrence Radiat. Lab., Rep. UCRL 7605 (1963).
13. T. Murase and A. R. McBirey, *Science* **170**, 165 (1970).
14. N. Warren, E. Schreiber, and C. Scholz, *Proc. Lunar Sci. Conf., 2nd, Geochim. Cosmochim. Acta* Suppl.. 2, **3**, 2345 (1971).*
15. K. Horai, G. Simmons, H. Kanomori, and D. Wones, *Proc. Apollo 11 Lunar Sci. Conf.; Geochim. Cosmochim. Acta* Suppl. 1, **3**, 2243 (1970).†
16. R. A. Robie and B. S. Hemingway, *Proc. Lunar Sci. Conf., 2nd, Geochim. Cosmochim. Acta* Suppl. 2, **3**, 2361 (1971).
17. R. A. Robie, B. S. Hemingway, and W. H. Wilson, *Proc. Apollo 11 Lunar Sci. Conf., Geochim. Cosmochim. Acta* Suppl. 1, **3**, 2361 (1970).
18. J. A. Bastin, P. E. Clegg, and G. Fielder, *Proc. Apollo 11 Lunar Sci. Conf., Geochim. Cosmochim. Acta* Suppl. 1, **3**, 1987 (1970).
19. K. Watson, I. The Thermal Conductivity Measurements of Selected Silicate Powders in Vacuum from 150°–350°K; II. An interpretation of the Moon's Eclipse and Lunation Cooling as Observed through the Earth's Atmosphere from 8–14 Microns. Ph.D. Thesis, California Inst. of Technol., Pasadena, 1964.
20. P. E. Clegg, J. A. Bastin, and A. E. Gear, *Mon. Not. Roy. Astron. Soc.* **133**, 66 (1966).
21. R. L. Wildey, *J. Geophys. Res.* **72**, 4765 (1967).
22. A. E. Wechsler and P. E. Glaser, Thermal Conductivity of Non-Metallic Materials. A. D. Little, Inc., Cambridge, Massacuhsetts, Rep. NASA Contract NAS8-1567 (1964).
23. A. E. Wechsler and M. A. Kritz, *Proc. Therm. Conductivity Conf., 5th, Univ. Denver* p. II-D-1 (1965).
24. A. E. Wechsler and I. Simon, Thermal Conductivity and Dielectric Constant of Silicate Materials. A. D. Little, Inc., Cambridge, Massachusetts, Rep. NASA Contract No. NAS8-20076 (1966).
25. H. S. Carslaw and J. S. Jaeger, "Conduction of Heat in Solids," p. 334. Oxford Univ. Press, London and New York, 1959.
26. J. H. Blackwell, *Can. J. Phys.* **34**, 412 (1956).
27. J. A. Fountain and E. A. West, *J. Geophys. Res.* **75**, 4063 (1970).
28. J. C. Mulligan, *J. Geophys. Res.* **75**, 4180 (1970).
29. C. J. Cremers, *Rev. Sci. Instrum.* **42**, 1694 (1971).
30. E. C. Bernett, H. L. Wood, L. D. Jaffee, and H. E. Martens, *AIAA J.* **1**, 1402 (1963).
31. P. A. Ade, J. A. Bastin, A. C. Marston, S. J. Pandya, and E. Puplett, *Proc. Lunar Sci. Conf., 2nd, Geochim. Cosmochim. Acta* Suppl. 2, **3**, 2203 (1971).
32. C. J. Cremers, R. C. Birkebak, and J. P. Dawson, *Proc. Apollo 11 Lunar Sci. Conf., Geochim. Cosmochim. Acta* Suppl. 1, **3**, (1970).
33. A. P. Vinogradov, *Proc. Lunar Sci. Conf., 2nd, Geochim. Cosmochim. Acta* Suppl. 2, **1**, 10 (1971); also in *J. Brit. Interplanet. Soc.* **24**, 475–495 (1971).

* Published by MIT Press, Cambridge, Massachusetts.
† Published by Pergamon, New York.

34. V. S. Avduevskii, N. A. Anfimov, M. Y. Marov, S. P. Shalaev, and S. P. Ekonomov, *Sov. Phys.—Dokl.*, **16**, 55 (1971).
35. M. G. Langseth, Jr., S. P. Clark, Jr., J. Chute, Jr., and S. Kerhm, *Rev. Abstr. Lunar Sci. Conf., 3rd* Lunar Sci. Inst., Houston, Contrib. No. 88, p. 475 (1972).
36. M. G. Langseth, Jr., A. E. Wechsler, E. M. Drake, G. Simmons, S. P. Clark, Jr., and J. Chute, Jr., *Science* **168**, 211 (1970).
37. C. J. Cremers and R. C. Birkebak, *Proc. Lunar Sci. Conf., 2nd, Geochim. Cosmochim. Acta* Suppl. 2, **3**, 2311 (1971).
38. C. J. Cremers, *AIAA J.* **9**, 2180 (1971).
39. C. J. Cremers, R. C. Birkebak, and J. E. White, *Int. J. Heat Mass Transfer* **15**, 1045 (1972).
40. C. J. Cremers, *Moon* **4**, 88 (1972).
41. C. J. Cremers, *Icarus* **18**, 294 (1973).
42. C. J. Cremers, *Proc. Lunar Sci. Conf., 3rd, Geochim. Cosmochim. Acta* Suppl. 3, **3**, 2611 (1973).*
43. R. Fryxell, D. Anderson, D. Carrier, W. Greenwood, and G. Heiken, *Proc. Apollo 11 Lunar Sci. Conf., Geochim. Cosmochim. Acta* Suppl. 1, **3**, 2121 (1970).
44. W. D. Carrier, III, S. W. Johnson, R. A. Werner, and R. Schmidt, *Proc. Lunar Sci. Conf., 2nd, Geochim. Cosmochim. Acta* Suppl. 2, **3**, 1959 (1971).
45. T. Gold, M. J. Campbell, and B. T. O'Leary, *Proc. Apollo 11 Lunar Sci. Conf., Geochim. Cosmochim. Acta* Suppl. 1, **3**, 2149 (1970).
46. E. A. King, Jr., J. C. Butler, and M. F. Carman, *Proc. Lunar Sci. Conf., 2nd, Geochim. Cosmochim. Acta* Suppl. 2, **1**, (1971). 737
47. T. Gold, E. Bilson, and M. Yerbury, *Rev. Abstr. Lunar Sci. Conf., 3rd,* Lunar Sci. Inst., Houston, Contrib. No. 88, p. 318 (1972).
48. D. F. Winter and J. M. Saari, *Astrophys. J.* **156**, 1135 (1969).
49. B. S. Hemingway and R. A. Robie, *Rev. Abstr.* Lunar *Sci. Conf., 3rd,* Lunar Sci. Inst., Houston, Contrib. No. 88, p. 369.(1972).
50. H. Kanamori, N. Fugii, and H. Mizutani, *J. Geophys. Res.* **73**, 595 (1968).
51. H. Kanamori, H. Mizutani, and N. Fujii, *J. Phys. Earth* **17**, 43 (1969).
52. K. Horai, S. Baldridge, and G. Simmons, *Proc. Lunar Sci. Conf., 2nd, Houston,* 1971.
53. H. Mizutani, N. Fujii, Y. Hamano, and M. Osako, *Rev. Abstr. Lunar Sci. Conf., 3rd,* Lunar Sci. Inst., Houston, Contrib. No. 88, p. 549 (1972).
54. J. C. Jaeger, *Proc. Cambridge Phil. Soc.* **49**, 355 (1953).
55. W. M. Sinton, *in* "Physics and Astronomy of the Moon" (Z. Kopal, ed.), p. 407. Academic Press, New York, 1962.
56. R. W. Muncey, *Nature (London)* **181**, 1458 (1958).
57. J. Reichman, *AIAA Thermophys. Conf., 3rd, Los Angeles* AIAA Paper 68–746 (1968).
58. J. D. Halajian and J. Reichman, *Icarus* **10**, 179 (1969).
59. J. Ulrichs and M. J. Campbell, *Icarus* **11**, 180 (1969).
60. Earl of Rosse, *Proc. Roy. Soc., London* **17**, 436 (1869).
61. B. C. Murray and R. L. Wildey, *Astrophys. J.* **139**, 734 (1964).
62. F. J. Low, *Astrophys. J.* **192**, 806 (1965).
63. J. W. Lucas, J. E. Conel, and W. A. Hagemeyer, *J. Geophys. Res.* **72**, 779 (1967).
64. G. Vitkus, J. W. Lucas, and J. M. Saari, *AIAA Thermophys. Conf., 3rd, Los Angeles,* AIAA Paper 68–747 (1968).
65. G. Vitkus, R. R. Garipay, W. A. Hagemeyer, J. W. Lucas, and J. M. Saari, Lunar Surface Temperatures and Thermal Characteristics, Surveyor VI A Preliminary Report. *NASA Spec. Publ.* **NASA SP-166**, 97 (1968).

66. G. Vitkus, R. R. Garipay, W. A. Hagemeyer, J. W. Lucas, B. P. Jones, and J. M. Saari, Surveyor VII A Preliminary Report. *NASA Spec. Publ.* **NASA SP-173,** 163 (1968).
67. L. D. Stimpson and J. W. Lucas, *AIAA Thermophys. Conf., 4th, San Francisco* AIAA Paper 69–594 (1969).
68. F. S. Johnson, *J. Meterol.* **11,** 431 (1959).
69. M. Baker, *Opt. Spectra* **6,** 32 (1972).
70. C. J. Cremers, R. C. Birkebak, and J. E. White, *AIAA J.* **9,** 1899 (1971).
71. C. J. Cremers, R. C. Birkebak, and J. E. White, *Moon* **3,** 346 (1971).
72. J. M. Saari, *Icarus* **3,** 161 (1964).
73. H. C. Ingrao, A. T. Young, and J. L. Linsky, *in* "The Nature of the Lunar Surface" (W. N. Hess, D. H. Menzel, and J. A. O'Keefe, ed.), p. 185. John Hopkins Press, Baltimore, Maryland, 1966.